

Bilaterally Controlled Micromanipulation by Pushing in 1-D with nano-Newton Scale Force Feedback

Ahmet Ozcan Nergiz

Submitted to the Graduate School of Engineering and
Natural Sciences in partial fulfillment of the requirements for
the degree of
Master of Science



Mechatronics Program
Faculty of Engineering and Natural Science
Sabancı University
Turkey

January 2009

Dedicated to the God

Bilaterally Controlled Micromanipulation by Pushing in 1-D with nano-Newton Scale Force Feedback

Ahmet Ozcan Nergiz

Abstract

In this thesis the focus is on mechanical micromanipulation which means manipulation of micro objects using mechanical tools. Pushing is a type of motion of the micro parts and pushing ability on micro scale is inevitable for many applications such as micro assembly of systems or characterization of tribological properties of micro scale things. The aim of the work in this thesis was to obtain an improved performance in 1-D pushing of micrometer scaled objects in the sense of giving more control to human operator where it allows human intervention via bilateral control with force feedback in nano-Newton scale. For this purpose a system which can practice 1-D pushing of micrometer scaled objects by human operator is built. A bilateral architecture which is composed of master and slave sides has been used in the system. The micrometer scaled object is pushed by the piezoactuator which constitutes the slave side and the master side is a DC motor where the shaft is turned by the human operator via a rectangular prism rod. This system can be considered as an improved system comparing with the ones in literature, since it has a number of different advantages together. One of them is the ability to calibrate the relation between the movement of the slave system and the cycle that is made by the DC motor shaft which is controlled by the operator. This gives the availability to decide how sensitive will the slave side motion be to the master side motion. Moreover, thanks to the nano-Newton scale force sensing ability of the system user has the chance to use this as a force feedback within the bilateral structure, where by the way the operator will understand when the piezoresistive cantilever beam touched the object that is going to be pushed by it. The operator also understands when there is an obstacle or opposite force that keeps the object from continuing on its track.

Bilaterally Controlled Micromanipulation by Pushing in 1-D with nano-Newton Scale Force Feedback

Ahmet Özcan Nergiz

ÖZET

Bu tezde yoğunlaşılacak konu, mikrometre ölçütündeki nesnelere mekanik araçlar yardımıyla manipüle edilmesi anlamına gelen mekanik mikromanipülasyondur. "İtme", mikro nesnelere uygulanabilen bir devinim çeşididir. Mikro ölçütte itme yetisi, sistemlerin mikro montajı, mikro ölçütteki nesnelere tribolojik özelliklerinin karakterize edilmesi gibi birçok uygulamada gereklidir. Burada anlatılacak çalışmanın amacı mikro ölçütteki nesnelere bir boyutta itilmesi işleminde sağlanan performansı geliştirmektir. Bu gelişme, nano-Newton hassasiyetinde kuvvet geri besleme yetisine sahip çift taraflı kontrol vasıtasıyla insan faktörünün operatör olarak kontrol döngüsüne katılmasıyla sağlanmaktadır. Bu amaçla, mikrometre ölçütündeki nesnelere insan kontrolünde ve bir boyutta itilmesine imkân veren bir sistem inşa edilmiştir. Bu sistemde yöneten ve yönetilen kısımlardan oluşan çift taraflı bir yapı kullanılmıştır. Mikrometre ölçütündeki nesne yönetilen taraftaki piezo eyleyici tarafından itilmektedir. Yöneten tarafta ise mili insan tarafından döndürülerek kontrol edilen bir doğru akım motoru mevcuttur. Döndürme işleminde kolaylık sağlanması için motor miline dikdörtgen prizma şeklinde bir çubuk monte edilmiştir. Sağladığı çeşitli avantajlar sebebiyle bu sistem, literatürdeki muadillerine nazaran daha gelişmiştir. Bu avantajlardan biri, yönetilen sistemdeki piezo eyleyicinin yer değiştirme miktarı ile yöneten taraftaki doğru akım motorunun yaptığı döngü sayısı arasındaki ilişkinin derecelendirilebilmesidir. Böylece, yönetilen tarafın, yöneten taraftaki değişikliğe ne derecede hassas olacağı ayarlanabilir. Bunlara ek olarak, sistemin nano-Newton hassasiyetinde kuvvet ölçüm yetisi, kullanıcıya bunu çift taraflı yapı içerisinde geri besleme ögesi olarak kullanabilme olanağı vermektedir. Bu sayede yöneten taraftaki kullanıcı, yönetilen taraftaki eyleyicinin, itilecek olan mikro ölçütteki nesneye dokunduğu anı hissedebilme şansına sahip olmaktadır. Ayrıca nesnenin önünde herhangi bir engel ya da hareketini zorlaştıran karşı yönde bir kuvvet belirlediği zaman kullanıcı bunu hissedecek ve önlemini alacaktır.

Declaration

The work in this thesis is based on research carried out by the Microsystems Group, at the program of Mechatronics Engineering , Faculty of Engineering and Natural Sciences, Sabanci University, Istanbul, Turkey. No part of this thesis has been submitted elsewhere for any other degree or qualification and it all my own work unless referenced to the contrary in the text.

Copyright © 2009 by AHMET OZCAN NERGIZ.

“The copyright of this thesis rests with the author. No quotations from it should be published without the author’s prior written consent and information derived from it should be acknowledged” .

Acknowledgements

In this part, I would like to express my appreciation to people and organizations who supported me when I am trying to achieve the work I will be presenting within this thesis.

First of all, I must tell that I had an advisor which has always approached to me like a father more than an advisor. It was a gorgeaus experience to study with him since he is one of the wisest man I've ever seen not only as an academician but also as a person. So, Prof. Asif Sabanovic will be my source of inspiration during my remaining life.

I would also like to thank to Shahzad Khan, Ph.D., my partner during this work. We did everything together and I could always find his support as a friend and partner as I face with some obstacles that were not easy to overcome by myself.

I should also mention my gratitude to Assist. Prof. Volkan Patoglu and Assoc. Prof. Mustafa Unel, who did help to get through the bottlenecks in parts of the project that are related to their areas of research.

My special thanks are to Assoc. Prof. Ugur Sezerman who believed in me and opened a way for me to get supported by TUBITAK, ANKARA/TURKEY. Accordingly, thanks to TUBITAK, ANKARA/TURKEY, which financially supported this project.

Lastly, I want to thank to my family who were with me every second and who spent a great amount of effort to raise me to a point that I am proud of being at.

Contents

| | |
|---|------------|
| Abstract | iii |
| Declaration | iv |
| Acknowledgements | v |
| 1 Introduction | 1 |
| 1.1 Overview | 1 |
| 1.2 Problem Definition and Approach | 2 |
| 1.3 Contribution | 2 |
| 1.4 Outline of the Thesis | 3 |
| 2 State of the Art | 5 |
| 2.1 Definition of Microsystem | 5 |
| 2.2 Overview of the Field of Microassembly | 6 |
| 2.3 Micro-manipulation of the Objects | 7 |
| 2.3.1 Manipulation by Pushing | 8 |
| 2.4 Dominant Forces of Micro World that Affect the Manipulation Process | 8 |
| 2.5 Bilateral Control | 11 |
| 2.6 Conclusion | 12 |
| 3 Custom-Designed Micromanipulation Setup | 13 |
| 3.1 Introduction | 13 |
| 3.2 Custom Designed Mechanical Parts | 14 |
| 3.3 Modules of the System | 16 |
| 3.3.1 Actuator Modules | 16 |

| | | |
|----------|---|-----------|
| 3.3.2 | Force Sensing Modules | 18 |
| 3.3.3 | Visual Feedback Modules | 19 |
| 3.3.4 | Signal Processor Module | 19 |
| 3.3.5 | Master Module - Bilateral | 21 |
| 3.4 | User Interface | 22 |
| 3.5 | Conclusion | 23 |
| 4 | Nano-meter Precision Motion Control of PZT Actuator | 26 |
| 4.1 | Open Loop Control of PZT Actuator | 27 |
| 4.1.1 | Hysteresis in PZT and the Bouch-Wen Model that is Used | 27 |
| 4.1.2 | Implementation | 29 |
| 4.1.3 | Experimental Results | 31 |
| 4.2 | Closed-loop Position Control of PZT Actuator using Sliding Mode Controller | 32 |
| 4.2.1 | Sliding Mode Controller Design | 33 |
| 4.2.2 | Discrete Form | 35 |
| 4.2.3 | Disturbance Observer | 37 |
| 4.2.4 | Implementation on PZT and Experimental Results | 39 |
| 4.3 | Conclusion | 39 |
| 5 | Scaled Bilateral Teleoperation for Micro-manipulation by Pushing in 1-D | 43 |
| 5.1 | Nano-Newton Force Sensing | 44 |
| 5.1.1 | Experimental Results and Validation | 46 |
| 5.2 | Position/Force Tracking on Master and Slave | 46 |
| 5.2.1 | Experimental Results and Validation | 47 |
| 5.3 | Conclusion | 49 |
| 6 | Conclusion | 50 |
| 6.1 | Summary of the Thesis | 50 |
| 6.2 | Problems and Future Works | 51 |
| | Appendix | 59 |

| | |
|--|-------------|
| Contents | viii |
| A Tele-Micromanipulation Setup | 59 |
| B Nano-meter Precision Motion Control of PZT Actuator | 61 |

List of Figures

| | | |
|------|---|----|
| 2.1 | Graphical representation of the surface tension and the cohesive force balance among the inner liquid molecules | 9 |
| 2.2 | Capillary Action | 10 |
| 3.1 | Tele-Micromanipulation Setup | 14 |
| 3.2 | Custom built parts in the slave mechanism | 15 |
| 3.3 | Custom built parts in the master mechanism | 16 |
| 3.4 | a)PiezoMike: Piezoelectric Micrometer Drive b)NanoCube XYZ Piezo Nanopositioning Systems | 17 |
| 3.5 | E664 NanoCube Piezo Controller | 17 |
| 3.6 | a)AppNano Piezoresistive Cantilever with Wheatstone Bridge b)Cantilever Beam | 18 |
| 3.7 | a)Nikon MM-40 Tool Makers Microscope b)Unibrain Fire-i 400 Industrial Camera | 20 |
| 3.8 | DS1103 PPC Controller Board and Connector/LED Combi Panel . . | 21 |
| 3.9 | Master Mechanism | 22 |
| 3.10 | Maxon 4-Q-DC Servoamplifier | 22 |
| 3.11 | Maxon Choke Module | 23 |
| 3.12 | Position Control Layout | 24 |
| 3.13 | Bilateral Layout | 25 |
| 3.14 | Unibrain Fire-i Application | 25 |
| 4.1 | a)Piezo stack actuator illustration, b)Electromechanical model of PZT actuator | 30 |

| | | |
|-----|--|----|
| 4.2 | 1-PZT Amplifier, 2-Vibration Isolation Table, 3-Laser Controller, 4-Laser Head, 5-Three axis PZT actuator set, 6-Direction of movement | 32 |
| 4.3 | Results when sinusoidal voltage input is applied with a)Fixed frequency and varying amplitude, b)Varying frequency and fixed amplitude | 33 |
| 4.4 | Results when sinusoidal voltage input is applied with 1 Hz frequency and a)20 V amplitude, b)50 V amplitude, c)80 V amplitude | 34 |
| 4.5 | a)Reference tracking for sinusoidal input, b)Error of reference tracking for sinusoidal input | 41 |
| 4.6 | a) Position response for a reference of $50nm$ [1], b) Position response for a trapezoidal reference with height $0.5 \mu m$, c) Position response for a sinusoidal reference with $1\mu m$ amplitude and $1Hz$ frequency . . | 42 |
| 5.1 | Schematics of the bilateral system | 44 |
| 5.2 | Force Sensing Results a) Approaching mode b) Pull-off mode | 47 |
| 5.3 | a) Position and b) Force Tracking Results | 48 |

List of Tables

| | | |
|-----|---|----|
| A.1 | Maxon RE 40 DC Motor Data | 59 |
| A.2 | Maxon 4-Q-DC Servoamplifier Data | 60 |
| A.3 | Maxon Choke Module Technical Data | 60 |
| B.1 | Specifications of Piezo-Stage | 61 |

Chapter 1

Introduction

1.1 Overview

Beginning from the Prof. Richard P. Feynman's famous talk [2] called "There's Plenty of Room at the Bottom" in 1959, people started to look forward to manipulate matter on smaller scales. The source of this idea was the belief that matter can be manipulated on atomic scales, which will then pave a way to produce better technological instruments such as faster computers with denser circuitry, powerful microscopes that are used to take images on nanoscale or a robot that can penetrate into body and can be used as an in-vivo medical treatment tool. Following this trend, achievements in this area, today made micro and nano-scale manipulation possible to some extent either mechanically or by controlling self triggered chemical processes. That achievements include a better understanding of the physics on smaller scales and better tools that will help people to obtain experimental verification.

In this thesis the focus is on mechanical micromanipulation which means manipulation of micro objects using mechanical tools. Micro motion for the micro parts can be categorized in the following four groups [3]: Lift up (stick, hold, vacuum, non-contact etc.), Place (remove, stick to the object etc.), Arrange (lift up & place, rotate, slide etc.) and Push (hold, clamp, deform etc.). From within these motion types, "pushing" is of concern for this thesis. Pushing ability on micro scale is inevitable for many applications such as micro assembly of systems or characterization of tribological properties of micro scale things.

1.2 Problem Definition and Approach

The aim of the work in this thesis was to obtain an improved performance in 1-D pushing of micrometer scaled objects in the sense of giving more control to human operator where it allows human intervention via bilateral control with force feedback in nano-Newton scale. Several steps accomplished one after another, ordered regarding their necessities during the development of such a system that the pushing is performed by. First of all, high precision control problem of the motion is addressed, since pushing of micro objects at position scales down to nanometer was targeted. A closed loop sliding mode controller has been developed for this purpose. The next target was achieving 1-D force sensing in nano-Newton scale, which is reached by using a piezoresistive cantilever with inbuilt wheatstone bridge. Voltage signals coming from the wheatstone bridge is amplified and calibrated using the characteristics of piezoresistive cantilever to obtain the corresponding force signal. Then, this force signal is used as a feedback to the bilateral control mechanism that allows human intervention. Bilateral system is basically composed of master and slave sides, which are the dc motor module and the 3-axes piezo actuator system respectively.

1.3 Contribution

As a result of the step-by-step effort given in the order explained above, a system which can practice 1-D pushing of micrometer scaled objects by human operator is built. Since a bilateral architecture used in the system, the micrometer scaled object is pushed by the piezoactuator which constitutes the slave side and the master side is a DC motor where the shaft is turned by the human operator via a rectangular prism rod. This system can be considered as an improved system comparing with the ones in literature, since it has a number of different advantages together.

One of them is the ability to calibrate the relation between the movement of the slave system and the cycle that is made by the DC motor shaft which is controlled by the operator. By the way slower and smoother motion of the slave actuator can be obtained when user does calibration in a way that less distance is gone by the slave

actuator per the cycle made by the master actuator. High movement resolution of the actuator used at the slave side is also one of the factors that creates this advantage.

Moreover, thanks to the nano-Newton scale force sensing ability of the system user has the chance to use this as a force feedback within the bilateral structure, where by the way the operator will understand when the piezoresistive cantilever beam touched the object that is going to be pushed by it. The operator also understands when there is an obstacle or opposite force that keeps the object from continuing on its track. Again calibration can be done in a way that will make the system really sensitive where a really small force in nano-Newton scale can be transferred to the master side as a tangible force.

1.4 Outline of the Thesis

Here you can find the outline of the thesis which explains the organization of the thesis with abstract information about following chapters:

- **Chapter 2:** The definitions and short literature surveys of microsystems, micromanipulation and manipulation by pushing is presented in the first half of this chapter. Following part includes information about the dominant forces in micro-scale world and present state of art that bilateral control has.
- **Chapter 3:** This chapter includes information about the custom built tele-micromanipulation setup and its parts utilized for the work in this thesis.
- **Chapter 4:** In this part, high precision control methods for PZT actuators is presented. Firstly, open loop control and hysteresis compensation for open loop controller is explained. Then, closed loop control using sliding mode controller is given with experimental results.
- **Chapter 5:** In this chapter, force controlled 1-D pushing is demonstrated based on the nano-Newton scale force sensing with human intervention opportunity using bilateral control mechanism which is again presented in this chapter.

- **Chapter 6:** Thesis is being finalized with the summary along with the future works.

Chapter 2

State of the Art

The definitions and short literature surveys of microsystems, micro assembly process, micromanipulation and manipulation by pushing is presented in the first half of this chapter. Following part includes information about the dominant forces in micro-scale world that should be considered during manipulation and about present state of art that bilateral control has.

2.1 Definition of Microsystem

Microsystem term stands for the systems on micro scale. In other words, systems with dimensions on a scale of one millionth of a meter. Microsystem can also be defined as a small system built from a number of functional parts where the functionality ensured in case an object or a part of microsystem or an environment contacting with it are all in common time-space dynamics.

Typical sub-categories of microsystems can be listed as follows: sensitive elements and converters of information for physical magnitudes; executive devices such as micromechanisms, microtools; power and motion sources such as microdrives, microturbines; microelectromechanical, microoptomechanical and biotechnical microsystems, biochips, energy supply microsystems, technological microsystems.

Microsystems are fabricated using microfabrication and they stand as a single entity. One of the direct forward and advantageous way of the fabrication of microsystems is to assemble separate microcomponents [4].By this way optimal conditions

for each component can be obtained according to their functionality. Regarding the mechanical aspect of the process the term "microassembly" appears and it stands as a field itself.

2.2 Overview of the Field of Microassembly

Microassembly is basically the process that takes place during the creation of microsystems out of separate components. Gathering of these components could be done either by using serial assembly where the parts are put together one at a time regarding the conventional pick and place paradigm or by using parallel assembly where more than one parts put together simultaneously. Microassembly process is not an easy one since every step is governed by the rules of micro world which are physically different than the phenomena in the macro world since different types of forces are dominant. Moreover, at the micro scale structures are so small to see and so fragile to handle since they usually break at micro-Newton force range. This situation makes the microassembly process impossible to be done using bare eye and bare hand. This restriction was the reason behind the efforts to develop tools and methods that makes microassembly possible. This efforts also included the intention towards getting an automated process. During the second half of 90's different groups have contributed to this effort using high precision actuators and vision feedback [5–8]. Then came the awareness about the necessity of the force measurement which made the general effort settle around two focuses: methodology of the assembly force measurement and strategy for part assembly. Different approaches such as PVDF piezoelectric force sensing [9–12], vision based force sensing [13], AFM based force sensing [14] and piezoresistive cantilever beam based force sensing [15–17] are applied to the force measurement problem. Each of them has their unique advantages regarding the applications they are being used at.

2.3 Micro-manipulation of the Objects

Micro-manipulation is by definition, any type of interaction that will change the relative position and relation of micro scale entities through direct or indirect human operator control. Positioning, cutting, pushing, pulling, grabbing, releasing etc. can be given as examples of these type of interactions.

Approaches to micro-manipulation can be arranged under different groups regarding four different criteria. First of them is regarding the scale that the manipulation is originated. "Top-down" micro-manipulation starts from using the tools and manipulating the phenomena in macro scale and goes down to micro scale in the sense of the world manipulated. "Bottom-up" micro-manipulation starts from the atoms and molecules level manipulation and tends to create the expected change in micro scale mostly using the tools like AFM or STM. Second criteria of categorization is the spontaneity of the process. Manipulation could be realized via "self-assembly" process such as dielectrophoresis, where micro scale entities are assembled themselves as a result of an electro-chemical process. "Assembly by physical manipulation" is the other way where the manipulation is applied via physical tools by the operator. Third categorization measure is whether there is contact between the manipulation tool and the object being manipulated. Manipulation using an AFM probe tip can be given as an example to "contact" micro-manipulation. An example to "non-contact" manipulation method is the laser trapping where electrostatic forces or magnetic field forces are used. Fourth and the last property of the manipulation that leads to different sub-groups is the automaticity of the process. The process can be manual, semi-automatic, automatic or teleoperated. Manual process does not include any automation and all tasks are done by human operators. They use necessary magnification and handling tools to facilitate the process, but it is not enough to achieve reliable results when the process is really sensitive since the human capabilities of vision and sensing are limited. Semi-automatic process has both automated sub-tasks and human operator intervention where in an automatic process all the tasks, order of tasks and the parameters are defined before the process. Teleoperation is done via a man-machine interface, employing a human operator to control a remote task which is not reachable or not convenient to oper-

ate directly. Utilizing a setup with an interface that helps the operator to control and feel the remote task at the same time makes it possible to obtain a reliable manipulation of the remote sub-system.

2.3.1 Manipulation by Pushing

As mentioned in the previous chapter, micro motion for the micro parts can be categorized in four different groups [3]: Lift up (stick, hold, vacuum, non-contact etc.), Place (remove, stick to the object etc.), Arrange (lift up & place, rotate, slide etc.) and Push (hold, clamp, deform etc.). From these group, pushing has some advantages comparing to others. It is easier to program the process and it is easier to handle since it does not require harder capabilities like carrying or lifting of objects. Moreover, it is enough to access the workpiece from just one side which especially applies for this work, since the focus is on the one dimension pushing process. There exist a number of different works where the manipulation by pushing is put into practice [14, 18–21].

2.4 Dominant Forces of Micro World that Affect the Manipulation Process

Forces can be categorized under 4 main categories which are gravitational forces, electromagnetic forces, strong and weak nuclear forces. Intermolecular interaction forces are especially based on electromagnetic forces which include the electrostatic force and the combination of magnetic and electric forces in action between charges moving relative to each other.

Another parameter of categorizing the forces is the range they show dominance. For some ranges there are more than one dominant type of forces. Our range of interest is the range that the micromanipulation and micro-assembly takes place, namely distances less than $0.1mm$. In this range the dominant forces are the capillary force that is effective from a few nm up to $1mm$, electrostatic force that is effective above $0.3nm$ and the Van der Waals force that is effective between $0.3nm$

and $100nm$.

Capillary force

Capillary action causes surface tension [22] [23] at the surface of the liquid. The reason behind this tension is the attraction forces caused by the molecular interaction among the liquid molecules. The surface molecules which have their some part in contact with the liquid medium and the remaining part in contact with the outer medium (air, vacuum etc.) are attracted towards the liquid medium more than the outer medium because of the attraction force imbalance. This situation creates a tendency to reduce the surface area and meantime changes the shape of the surface in a way that it has an inward curvature. Figure 2.1 shows the graphical representation of the surface tension and the cohesive force balance among the inner liquid molecules.

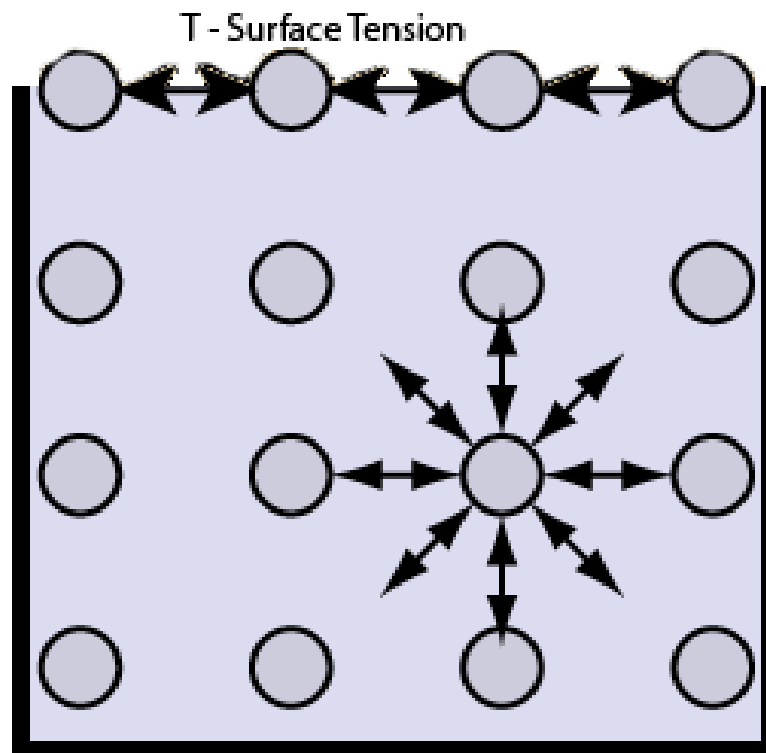
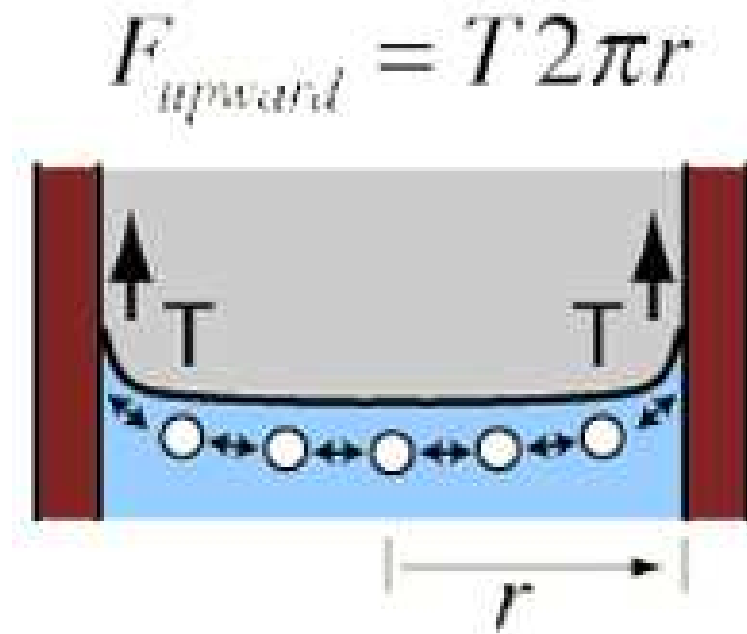


Figure 2.1: Graphical representation of the surface tension and the cohesive force balance among the inner liquid molecules

For a liquid in a tube, capillary action is observed when the adhesion force to the walls is more than the cohesive forces between the liquid molecules. Figure 2.2

illustrates this phenomena with the equation that accounts for the upward force.



T = surface tension

ρ = density of liquid

Figure 2.2: Capillary Action

Electrostatic Force

The fundamental relation expressing the force acting between two electric charges implies that the magnitude of the electrostatic force between two points' electric charges is directly proportional to the product of the magnitudes of all charges and the proportionality constant which is also known as Coulomb's constant. Force is inversely proportional to the square of the distance between the charges. Electrostatic forces arise from charge generation or transfer during contact.

Van der Waals Force

The van der Waals force is named after Dutch scientist Johannes Diderik van der Waals. It can create attraction or repulsion between molecules or between parts of the same molecule. However it is different than the forces due to covalent bonds or to the electrostatic interaction of ions with each other or with neutral molecules. Main

categories are permanent dipole-permanent dipole forces, permanent dipole-induced dipole forces and instantaneous induced dipole-induced dipole (London dispersion forces). They are relatively weak compared to normal chemical bonds.

2.5 Bilateral Control

”Bilateral” means ”which has two sides” and in the control perspective bilateral control can be created using two different systems called as master and slave sides which interact with each other and transfer real-time information to each other about the states they have. This method is usually employed when there is a need of communication and co-operation between two different systems that operates away from each other. The communication is provided by utilizing dedicated signal channels that transfer the measured data coming from one systems to another. Common applications include the haptic systems where human operator has to control a remote slave system with a capability of sensing the forces encountered by that system in its environment which is distant from the environment where human operator stands as the operator of master side. This is also called ”teleoperation”. Here, slave system moves depending on the position change data coming from the master side operated by human. However, the data comes scaled considering the range of the slave side actuator and the calibration needs depending on the application. Meantime, the human operator feels the forces encountered by the slave side via the calibrated force feedback from slave side towards master side.

Remote operation property is inevitable for some applications such as micro or nano meter scale manipulation. It is not possible for a human to directly manipulate objects in micro or nano meter scale environment since the scale that human can feel and see is much larger than the micro/nano meter scale. Utilizing teleoperation human obtain the ability to control the movement in micro/nano scale via controlling a system which is more convenient to operate directly. In literature, there exist a lot of different works on this subject [24–29].

Robust stability and transparency are two important and conflicting performance goals for teleoperation systems [30]. It is crucial to achieve loyal transmission of

signals (positions, velocities, forces) between master and slave. Ideally transparency means that the operator can feel like he/she is directly interacting with the remote task [31] which corresponds to slave side environment. However, it has been proved that this ideal case is not possible [32]. However, the expected practice is to approach the ideal case as much as possible when the system is being designed.

2.6 Conclusion

In this chapter, microsystems, micro assembly process, micromanipulation and manipulation by pushing are briefly explained. Then the dominant forces in micro-scale world that can not be negligible during manipulation are presented. Lastly, the area of bilateral control is summarized with some examples.

Chapter 3

Custom-Designed

Micromanipulation Setup

This chapter is included in the thesis to give information about the components of the custom designed micromanipulation setup developed as a part of the project and utilized for obtaining experimental results. ¹ Below a brief description of the setup is followed by the explanations and utilizations of home made parts of the mechanism. Then different functional parts of the system explained module by module. (i.e. actuation, force sensing, visual feedback, signal processing and master side of the bilateral mechanism) The chapter ends after a demonstration of user interface.

3.1 Introduction

Tele-Micromanipulation setup employed during this work is developed in a way that it supports the bilateral application. In other words, the structure has master and slave side mechanisms in addition to a human-computer interface module.(see Figure 3.1) An aluminum rod is connected to the shaft of a DC motor to obtain a master side mechanism that can be operated by human. Meantime a three axis piezo-stage that can be controlled through computer and dSpace 1103 module is employed

¹The figures used in this chapter are taken from the third chapter of the Ph.D. Thesis of Shahzad Khan, Ph.D., titled "Micromanipulation - A Force Feedback Approach", by courtesy of Shahzad Khan who also used the same micromanipulation setup for his study.

as the slave side mechanism since nano-meter accuracy in position control and nano-Newton scale force sensing was necessary. As implied by the bilateral structure, every change of position belongs to the human operated master side mechanism creates a scaled amount of movement of slave side mechanism.

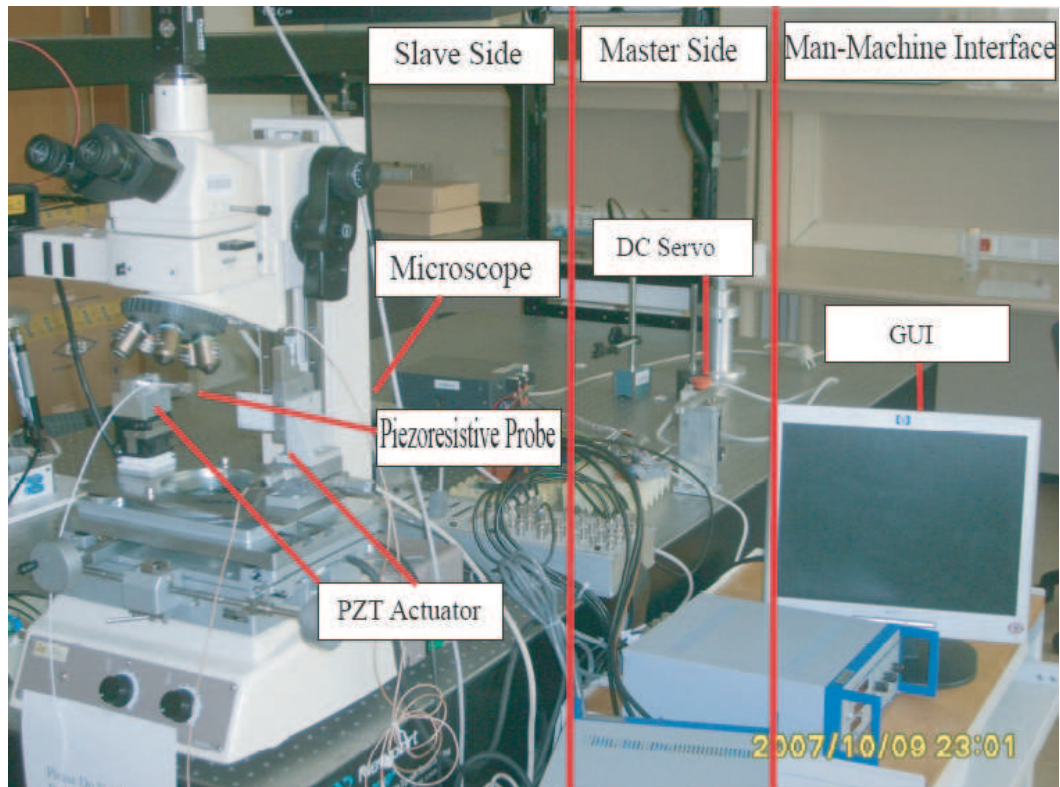


Figure 3.1: Tele-Micromanipulation Setup

3.2 Custom Designed Mechanical Parts

In Figure 3.2, home made parts in slave mechanism are depicted with labels on them. All of these parts are designed and fabricated for specific usage in this mechanism. AFM probe holder structure on the top left carries the piezoresistive cantilever in a convenient way by a rod that can turn 360 degrees around its central axis. The electrical connection cord of the cantilever is also tied to the cylindrical rod not to have difficulties with the cord. This structure is mounted on a 3-axes piezo-actuator, namely nanocube. On the right hand side exists the glass slide which has its upper edge at the same level of height with the piezoresistive cantilever. A plastic glass

slide holder is built and connected to the 3-axes open loop actuator mechanism. These three actuators are also connected to each other. They create the ability to set the level and position of the glass slide in a way that it can interact with the piezoresistive cantilever. Additional actuator holders are used to level the heights of the 2 different 3-axes actuator mechanisms since both mechanisms can move up to a certain range and this range is not enough to compensate the height difference between them. A base plate is placed at the bottom of everything since it was not convenient to use the uneven platform of the microscope. Base plate has a hole in the middle to let the bottom light pass through.



Figure 3.2: Custom built parts in the slave mechanism

For the master mechanism an aluminum DC motor holder structure that can be screwed on top of the vibration isolation table is built.(see: Figure 3.3) This structure carries the motor in a way that its shaft looks upwards. This was required since a rectangular prism shaped aluminum rod is connected to the shaft in order to turn it in a convenient way.

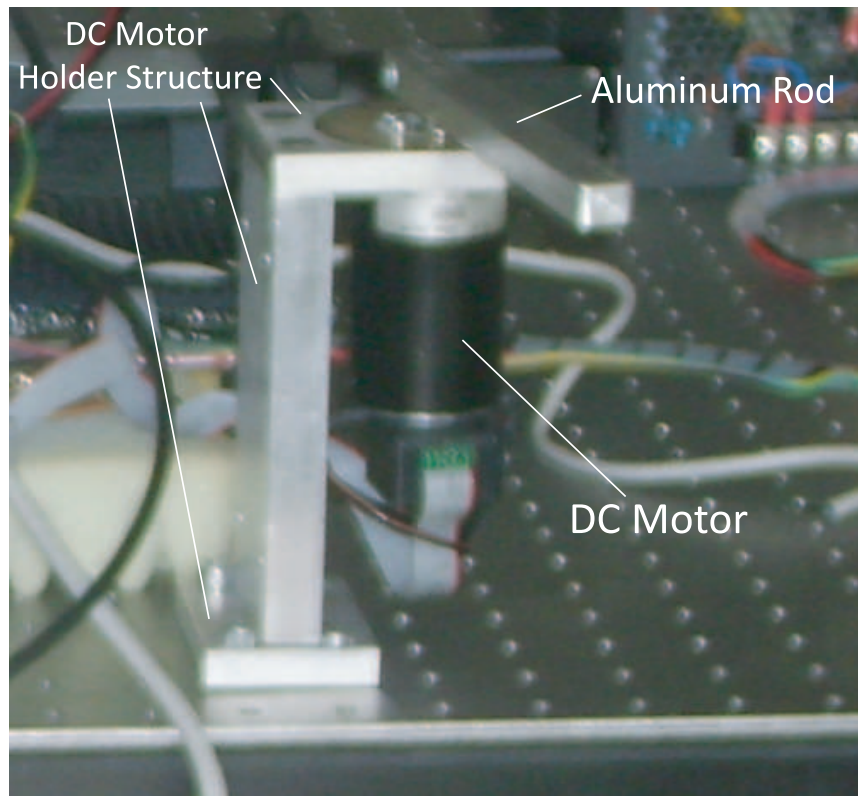


Figure 3.3: Custom built parts in the master mechanism

3.3 Modules of the System

3.3.1 Actuator Modules

Two different actuator modules are used for the positioning purposes of the Piezo-resistive micro cantilever and glass slide.

The one which is employed for the glass slide is composed of three stages of open loop actuators that are used together to obtain 3-axes movement. Physik Instrumente's P-854 piezoelectric micrometer drives which are integrated with high-resolution piezo linear drives has been utilized to move the glass slide and its holder structure in 3-axes.(see: Figure 3.4) The sensitivity of their manual operation is $1\mu m$. The micrometer tip can also be automatically moved in and out (up to $25\mu m$) relative to the manually set position by controlling the piezo voltage. Piezoelectric motion of these actuators has a resolution in the sub-nanometer range. During the experiments of this project, these actuators are operated only manually.

The second actuator module in the system is Physik Instrumente's XYZ Nano

Alignment system P-854 Nanocube (see: Figure 3.4, which is used for positioning of Piezo-resistive microcantilever. Here it works as a closed loop actuator which has a movement range of $100\ \mu\text{m}$ on each of three axes. Moreover it has a zero-stiction, zero-friction guiding system.



Figure 3.4: a) PiezoMike: Piezoelectric Micrometer Drive b) NanoCube XYZ Piezo Nanopositioning Systems

Physik Instrumente's E664 *NanoCube*[®] Piezo Controller is used with the system as an amplifier and position servo-controller. (see: Figure 3.5) During the operation, closed-loop external control mode was active. In this mode position change of PZT is controlled by an analog signal input ranges from 0 to +10 V. After the calibration of the controller, 10 V and 0 V inputs correspond to maximum nominal displacement and zero displacement respectively.



Figure 3.5: E664 NanoCube Piezo Controller

3.3.2 Force Sensing Modules

A piezoresistive cantilever with inbuilt wheatstone bridge is utilized to obtain force measurement which is used as the force feedback from the slave side of the bilateral structure. Cantilever has a resistance itself and stands as one of the resistors in the Wheatstone bridge. When the cantilever is deflected from its original position, a change occurs in its resistance. Accordingly, the output voltage of the Wheatstone bridge changes and this voltage is amplified by a wide bandwidth strain gage input module in order to get it within a range that it can be given as an input to the dSpace 1103 ppc controller board. This board sends the data to the computer. Using the geometry and characteristics of the cantilever beam along with the rules and assumptions that governs the relation between the beam deflection and the force applied on it, a force value is obtained which is used as the force feedback.

Figure 3.6 part a) shows the piezoresistive cantilever with Wheatstone bridge which is a product of Applied Nanostructures. It has a sensitivity of $5 \times 10^{-7} / \text{Angstrom}$. Depending on its leg dimensions the resistance can have a value between 900Ω and $2 \text{ K } \Omega$. The one used in this work has a base resistance of $1.2 \text{ K } \Omega$. For every $5 \mu\text{m}$ bending, 25Ω resistance change is observed. The dimensions of the cantilever are $300 \mu\text{m}$, $50 \mu\text{m}$ and $2 \mu\text{m}$ as length, width and thickness respectively. The tip height is $5 \mu\text{m}$.

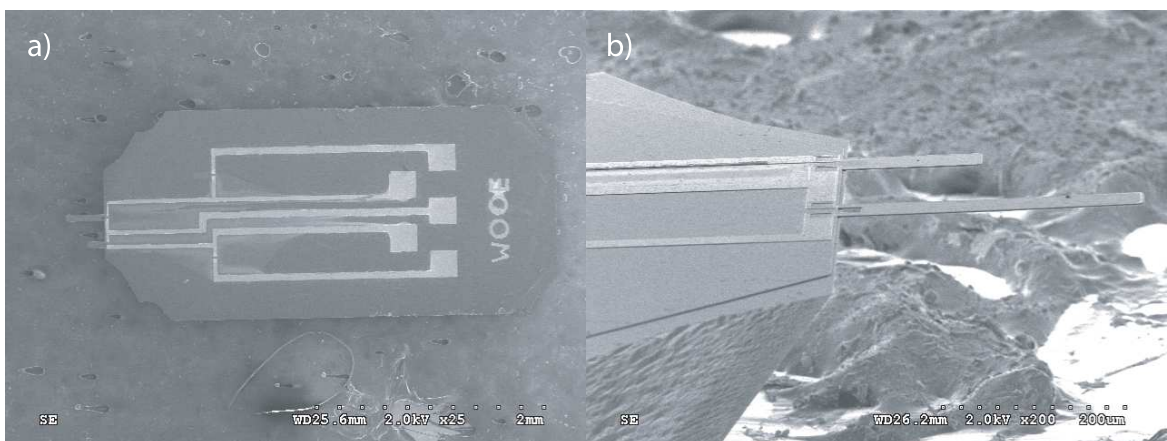


Figure 3.6: a) AppNano Piezoresistive Cantilever with Wheatstone Bridge
b) Cantilever Beam

Figure 3.6 part b) has a closer view of the cantilever beam. The longer beam is

piezoresistive and its tip is on the face that looks bottom.

As stated above output voltage coming from the wheatstone bridge needs amplification before being used as an input to dSpace 1103 ppc controller board. The reason is the input range of the A/D converter of the board which is ± 10 Volts. Dataforth SCM5B38-05D Wide Bandwidth Strain Gage Input Module is employed for this task. It has a voltage input range up to ± 20 mV and an output range up to ± 10 V. Its excitation voltage and the sensitivity are 10V and 2 mV/V respectively.

3.3.3 Visual Feedback Modules

A Nikon MM-40 Tool Makers Microscope along with a Unibrain Fire-i 400 Firewire Camera are used to capture the motion in the slave side and to transfer it to the computer.

The microscope (see Figure 3.7 part a)) has 5 different magnification objectives ranges between 5x and 100x. For this project, objectives up to 20x magnification could be used since the working distances of 50x and 100x magnifications make it impossible to do imaging without touching the parts of piezoresistive probe under the microscope. The coaxial x-y stage of the microscope where actuator modules are mounted upon, can move 150 mm on x axis and 100 mm on y axis. The objectives can move on z-axis with 150 mm range. Illumination is obtained using the top and bottom lights.

The firewire camera (see Figure 3.7 part b) that is connected to the computer is utilized mainly for capturing the image obtained through microscope with frame rates between 3.75 and 30 frames per second. It is a color industrial camera with a 640 x 480 pixels picture size.

3.3.4 Signal Processor Module

Signal processing task has been fulfilled using the dSpace 1103 ppc controller board. It stands as a communication unit between the computer which is the main control and processing station and the peripheral devices in the system. It makes the necessary conversions before transferring the signals from devices to computer and

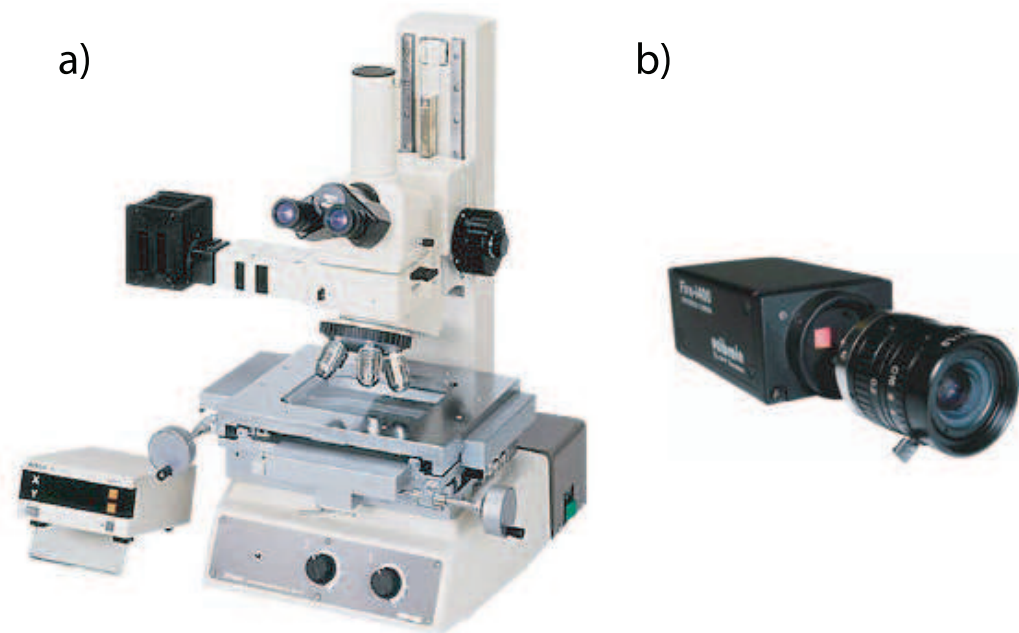


Figure 3.7: a)Nikon MM-40 Tool Makers Microscope b)Unibrain Fire-i 400 Industrial Camera

vice versa. Value of a signal passing through any channel can be assigned to a variable created by the user and can be monitored and manipulated using the coding interface that dSpace provides.

For this project 4 A/D, 4 D/A channels and an incremental encoder interface is utilized. Amplifier that gets the signal comes from the wheatstone bridge is connected to an A/D channel. DC servoamplifier of the DC motor used in master side of the bilateral structure is connected to a D/A channel. The encoder of the same motor is connected to the incremental encoder interface. In addition to these, E-664 piezo controller module occupies 3 A/D and 3 D/A channels for position encoding and actuation purposes of the *NanoCube*[®] on each axis.

Figure 3.8 depicts the dSpace1103 board and its enclosure which has the connections to channels of the board. Each connection has its own light emitting diode (LED) indicator light.

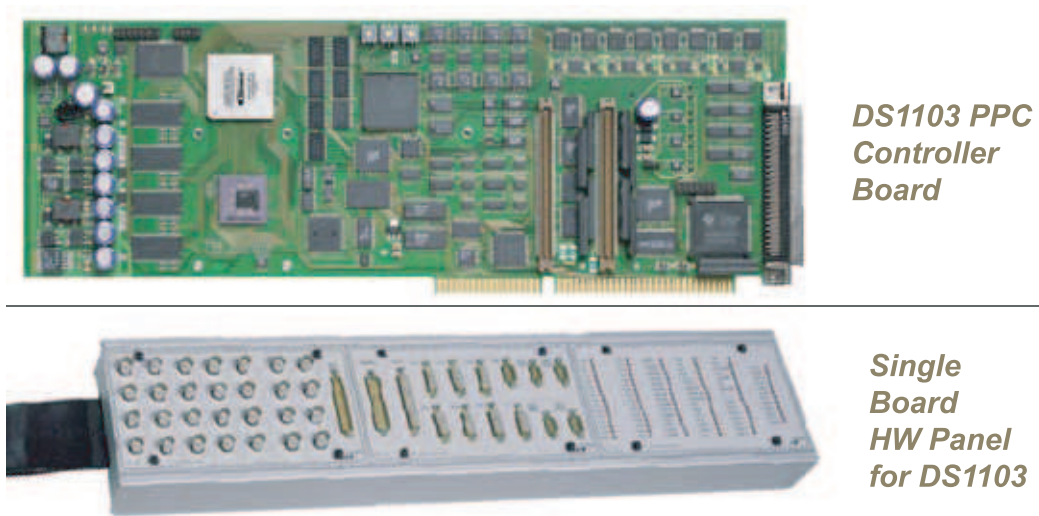


Figure 3.8: DS1103 PPC Controller Board and Connector/LED Combi Panel

3.3.5 Master Module - Bilateral

In the context of the bilateral structure used in this project the master side is basically composed of the Maxon RE-40 DC motor (see Figure 3.9), a Maxon 4-Q-DC servoamplifier (see Figure 3.10) that works with the motor and a Maxon choke module (see Figure 3.11) which is utilized to get a higher motor terminal inductance in order to get rid of the voltage ripple. A rectangular prism shaped rod is connected to the shaft of the DC motor to make it easily turnable by human hand.

The position change data of the DC motor shaft is transferred to the computer by the encoder signal processed through dspace1103 signal processor module. The force feedback from the slave side is reflected to the master side by the current signal again processed through the dspace1103 and given to the DC motor in order to create a motion opposite to the direction that human turns it when there is a repulsion against the piezoresistive cantilever tip. When there is an attraction force applying on the cantilever tip, current signal that comes to the DC motor makes it turn towards the same direction with human operator.

Tables A.1, A.2 and A.3 contain the technical data about the dc motor, the servoamplifier and the choke module respectively.

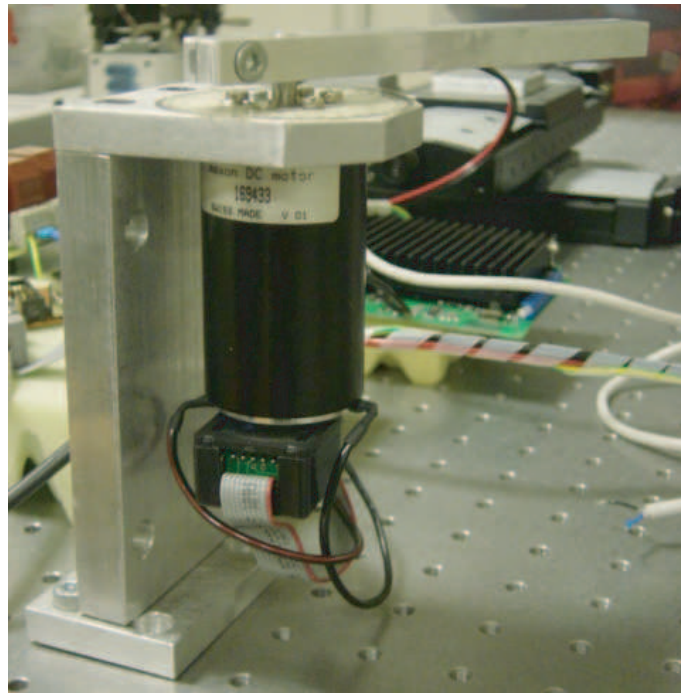


Figure 3.9: Master Mechanism

3.4 User Interface

ControlDesk environment of the dSpace is utilized as the user interface for control and measurement tasks since all of the signals between computer and devices are transferred through dSpace controller board. It is an easy to use software that works based on the work spaces created for each project. The codes that will work behind (for the purposes of parameterizing and processing the signals) can be written in C language. Layouts can be created as graphical interfaces that allows one to modify

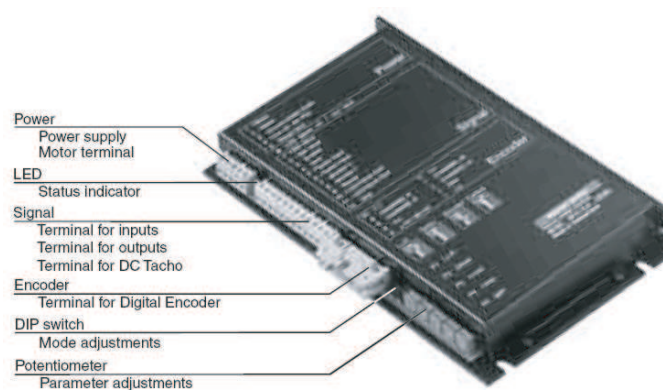


Figure 3.10: Maxon 4-Q-DC Servoamplifier

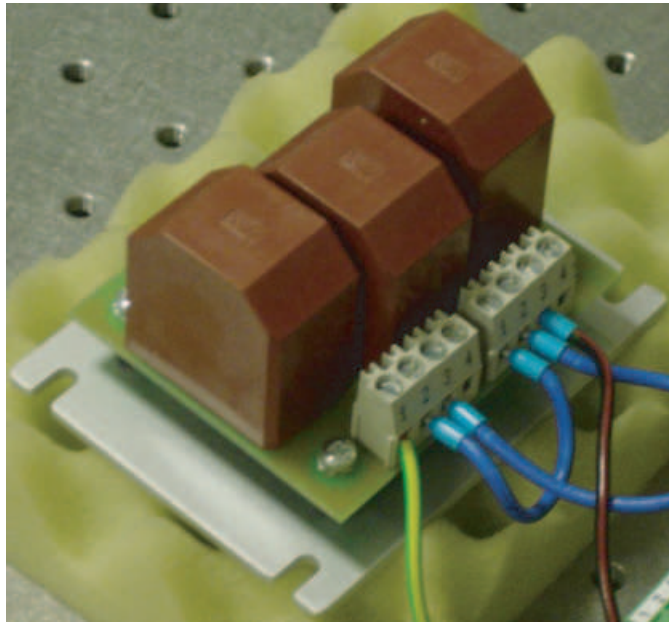


Figure 3.11: Maxon Choke Module

and monitor the parameters each of which created based on the signals processed through the controller board.

Figures 3.12 and 3.13 shows two layout examples that are used in this project.

Aside from the control and measurement purposes an interface was necessary for visual capturing and recording purposes. It is an inevitable part of the human interface since the operator has to have a real time vision of what is happening on the slave side when he/she is manipulating the system. Unibrain Fire-i application which is compatible with the utilized firewire camera is used as capturing interface. Figure 3.14 shows the graphical interface of the software. From here one can modify the pixel format, resolution and the frame rate.

3.5 Conclusion

This chapter has covered the explanations about the components that constitute the custom made micromanipulation setup which is built as a part of the project and used for the project. Moreover, information about how that components interact with each other was given when necessary. The tasks and specifications of each component is necessary to be understood well in order to figure out how the results

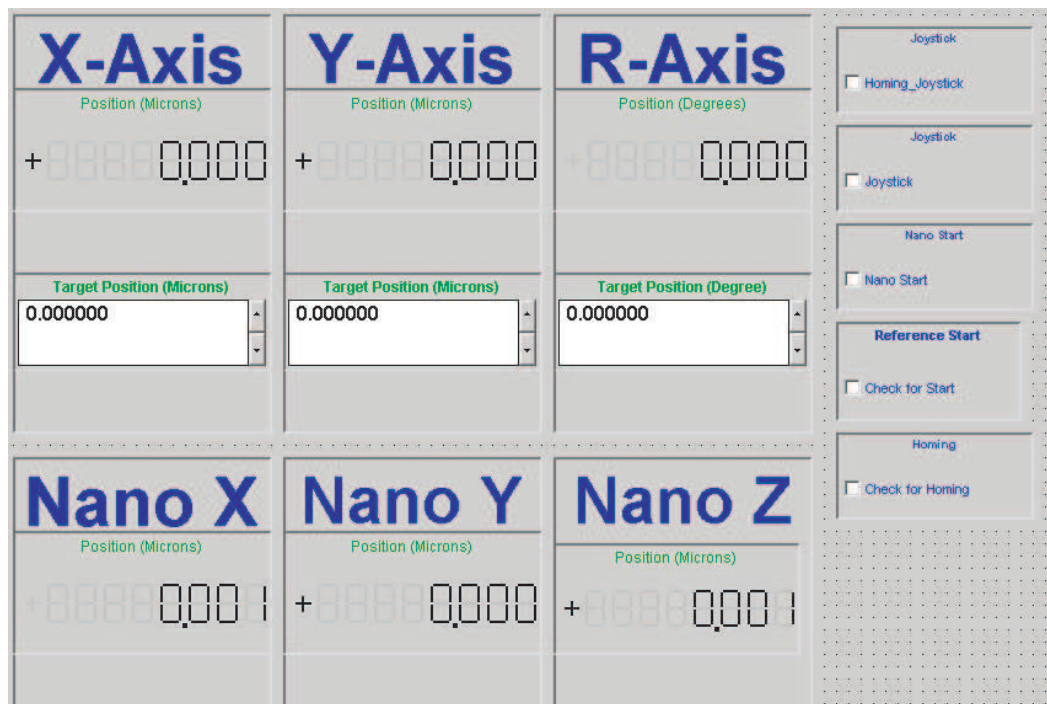


Figure 3.12: Position Control Layout

of the experiments could be obtained and how reliable they are.

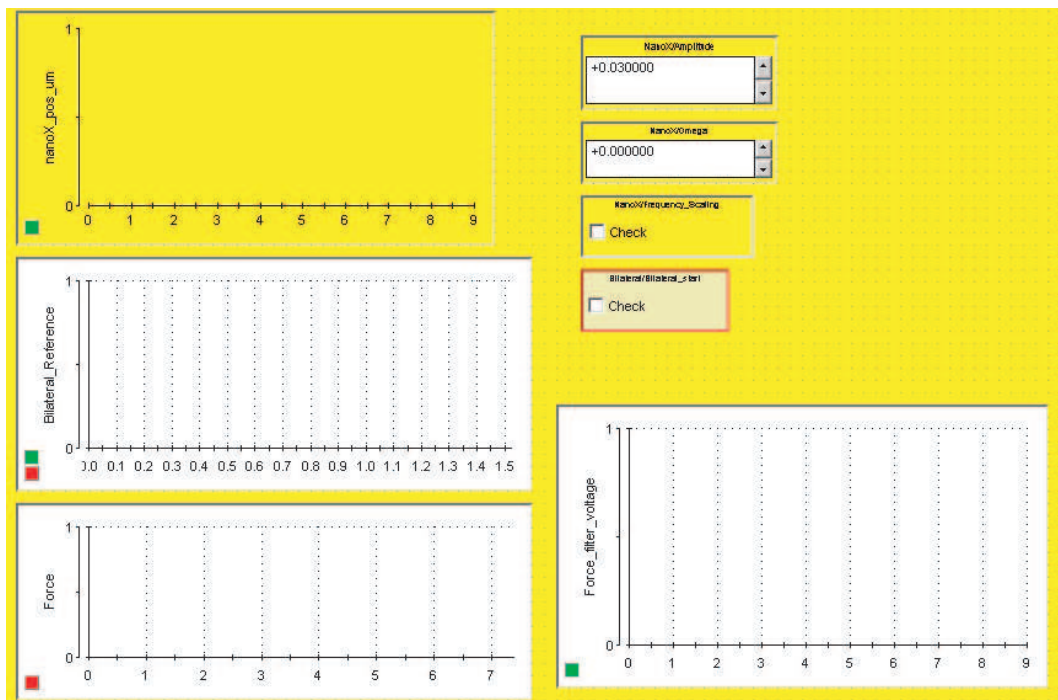


Figure 3.13: Bilateral Layout

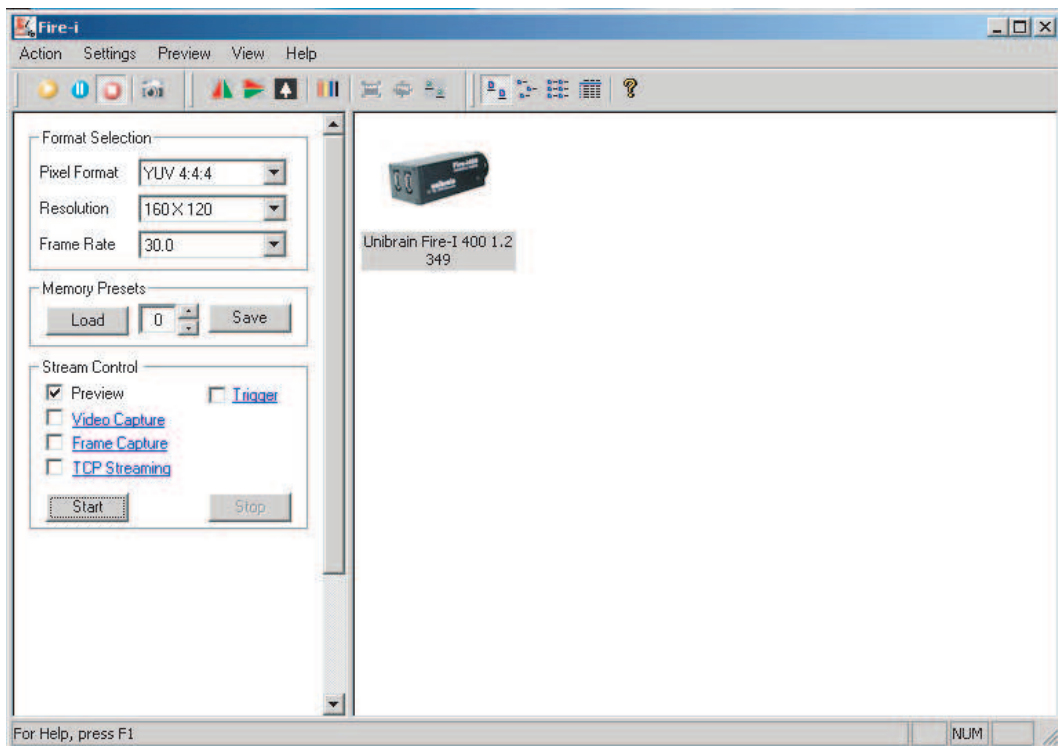


Figure 3.14: Unibrain Fire-i Application

Chapter 4

Nano-meter Precision Motion Control of PZT Actuator

For this project, nano-meter precision motion control was an inevitable need for obtaining a successful micromanipulation experience which was one of the targeted areas to improve. It was already known that the range of motion will go down to nano-meters and this motion had to be smooth and without any overshoot not to create a damage on the micro-objet/micro-manipulator couple.

In addition to the performance requirements stated above, uncertainties existing in the real world that can be gathered under 4 main categories (parametric uncertainty, actuator/sensor nonlinearities such as hysteresis, backlash in gear trains, time delay) make it hard to obtain high-precision motion control by just applying a classic PID controller and by eliminating the nonlinearities using the integral action. Instead, a discrete sliding mode controller with a disturbance observer has been modeled and implemented for this project.

This chapter explains the development process starting from the open loop control efforts resulted with successful compensation of the hysteresis that exists in the piezoactuator. Then comes the explanation of the closed loop control scheme which includes the sliding mode controller.

4.1 Open Loop Control of PZT Actuator

As the first step, open loop control of the utilized PZT actuator is chosen. In the context of control, "open loop" means that, in the control scheme there is no feedback from the actuator which is being controlled. In other words, control mechanism tries to get the actuator to the targeted position but no information about the position of the actuator is fed back to the control mechanism. That's why the control mechanism cannot calculate and use the info of how close could actuator go to the reference position. However it does not mean that the final position of the actuator is not being measured. That information is necessary for the operator to compare with the expected final position and to understand the performance of the controller.

PZT stack actuator is chosen as the type of actuator since it is able to perform step movements with nano-meter resolution and bandwidth that has the order of kilohertz. Moreover, since PZT stack actuator is monolithic it has no sliding or rolling parts which could create mechanical stiction or backlash. Its movability is based on the piezo-electricity. Which is a property of the material that allows to create electromechanical energy conversion. It is a bidirectional relationship between the electric charge and the mechanical deformation on the piezoelectric material. Application of one creates the other on the material and these phenomena are called piezo-electric effect and inverse piezo-electric effect where they mean the creation of electric charge under applied deformation and vice-versa respectively.

4.1.1 Hysteresis in PZT and the Bouch-Wen Model that is Used

By definition, hysteresis is a phenomenon wherein two (or more) physical quantities bear a relationship which depends on prior history. More specifically, the response Y takes on different values for an increasing input X than for a decreasing X. In our case, Y is the output position of the PZT actuator and the X is the input voltage given to the actuator.

Hysteresis loops happen when the system is wiggled back and forth again and

again. A system that has hysteresis may be in any number of states, regardless of the inputs to the system. For such a system, it is not possible to predict the output (i.e. the state of the system for a given input) without looking at the history of it. In order to make a prediction, one must look at the path followed by the output before reaching current value.

PZT actuator has the hysteresis as a non-linearity which is inherent. Regarding the definition above this non-linearity is rate-independent. This non-linearity has to be taken into account when the control is being designed. Otherwise instability may occur [33]. First of all hysteresis in the system must be modeled and then the input voltage must be modified using the inverse of the modeled hysteresis. The more accurate hysteresis model provides the more effective hysteresis canceling.

There are several different modeling approaches in the literature. One of them is modeling hysteresis as a nonlinear differential equation which is also known as Duhem-Madelung's model [34]. Another approach is modeling as a weighted superposition of many elementary hysteresis operators. Preisach type [35], Krasnoselski-Pokrovski type [36] and Ishlinski type [37] models are of this kind. A third different model is called as PEA [38] where hysteresis is proposed as a nonlinear resistive capacitive element in the electrical domain via Generalized Maxwell Slip [39]. All of these models stated above have some common drawbacks. Hysteresis loops produced by these models are mainly anti-symmetric and different from the experimental behavior of the piezoelectric actuators. In addition to this, they do not consider the effect of piezoelectric actuator's initial charges and initial strain. In other words they assume that the actuators are in the relaxed state before application of the input voltage [38]. These restrictions of the models come along with the uncertainty about resultant model's efficiency on reproduction of the all major and minor hysteresis loops.

The model used for this project is known as Bouch-Wen model [40] which was also successfully utilized as a hysteretic isolator by other people such as Constantinou [41], and Heine [42]. This model is successful when it comes to characterize the dynamics of mechanical systems since it is represented by a mass-spring-damper form differential equation. Moreover it does not suffer from the above mentioned

drawbacks as much as the other models stated before.

The model had to have a mathematical definition in order to be able to get integrated with the system dynamics and the Bouch-Wen model is defined by the equation below.

$$\dot{z} = \alpha\dot{x} - \beta|\dot{x}|z|\dot{z}|^{n-1} - \gamma\dot{x}|z|^n \quad (4.1)$$

Here, restoring force amplitude is set by parameter α . The shape of hysteresis loop and elastic to plastic response transition smoothness are tuned by the parameters β and γ . When we assume that the structure only responds elastically, the parameter n can be set equal to 1. By the way the Eqn.(4.1) reduces down to Eqn.(4.2).

$$\dot{z} = \alpha\dot{x} - \beta|\dot{x}|z - \gamma\dot{x}|z| \quad (4.2)$$

Here x is the state variable and z is the excitation which in our case correspond to displacement and voltage respectively.

4.1.2 Implementation

In order to use the model stated above, first of all the mathematical model of the PZT stack actuator has to be constructed. Figure 4.1 b) depicts the model used. Piezoelectric effect is taken separated from the hysteresis effect. T_{em} is the electromechanical transducer that represents the piezoelectric effect. The hysteresis effect is represented by H . u_p and u_h are the voltages due to piezo effect and hysteresis effect respectively where u_{in} is the total voltage over the PZT stack actuator. Since PZT stack is composed of wafers which are connected in parallel (See Figure 4.1 a)), the combined capacitance of the stack is the sum of the capacitances of the wafers and is represented by C_e . Since the sum of the charges on the PZT actuator is represented by q , the total current is represented by \dot{q} which is the time derivative of the charge. PZT actuator's length change as a result of the forces applied on it and this change is denoted by x . The forces are the transducer force represented by F_p and the external force represented by F_{ext} . Regarding the electromechanical

conversion electrical and mechanical energy are equal at the interaction ports. This is explained by the equation $u_p q_p = F_p x$.

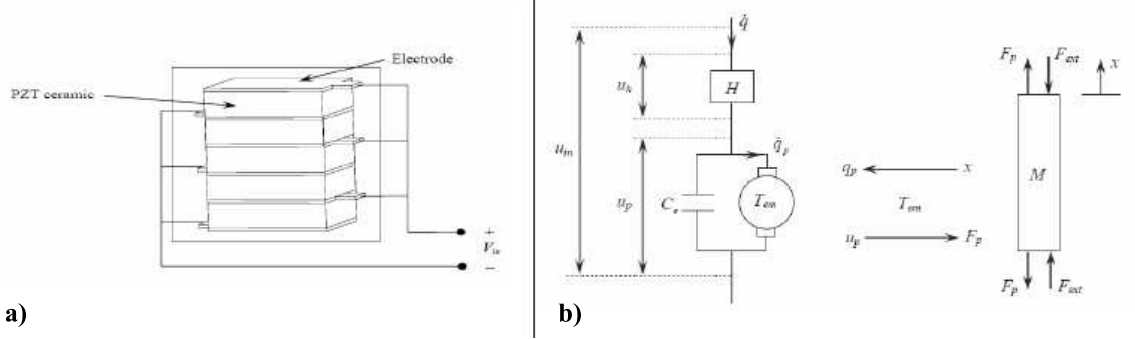


Figure 4.1: a) Piezo stack actuator illustration, b) Electromechanical model of PZT actuator

Effective mass, effective stiffness and damping co-efficient of the PZT actuator (m_p , k_p and c_p respectively) which are necessary for the electromechanical model, can be calculated using the following equations,

$$\begin{aligned} m_p &= \rho A_p L \\ k_p &= \frac{\rho A_p}{L} \\ c_p &= \frac{\eta A_p}{L} \end{aligned} \quad (4.3)$$

where E is the elasticity modulus of piezoelectric ceramic, η is the viscosity, ρ is the mass density, L is the length of PZT actuator and A_p is the cross-sectional area of PZT actuator.

The equation that involves the electromechanical structure is constructed as below:

$$m_p \ddot{x} + c_p \dot{x} + k_p x = T_{em}(u_{in}(t) - H(x, u_{in})) - F_{ext} \quad (4.4)$$

Where $H(x, u_{in})$ is the hysteresis function which has the displacement of the stage (x) and the total voltage on the PZT stack actuator (u_{in}) as parameters. Specifications of the piezoelectric actuator can be found in appendix. (See: Table B.1)

In order to combine the electromechanical model of the actuator with the hysteresis model obtained before, the variable z in Eqn.(4.2) is introduced into Eqn.(4.4). The combined version can be written as below:

$$m_p \ddot{x} + c_p \dot{x} + k_p x = T_{em} u_{in}(t) - T_{em} z - F_{ext} \quad (4.5)$$

Verification of the model has been done using a piezoelectric micrometer drive (P-854 of Physik Instrumente, Germany) that has integrated high resolution linear drives. Manual operation resolution of these drives is 1 micrometer. They can also be moved automatically by controlling the input voltage up to a 25 micrometer range back or forth depending on the set position before movement. Piezoelectric motion resolution is less than a nanometer. dSpace 1103 controller board is used as an interface that takes the digital signal coming from the computer and transfers it to the driver of the piezo actuator after converting it into an analog signal through its DAC module.

Displacement data is acquired by utilizing a laser interferometer (LK-2001 of Keyence) that has a CCD light receiver, enabling high accuracy and 1 micron resolution. dSpace 1103 is again used as an interface that takes the analog signal coming from the interferometer and transfers it to the computer after converting it into a digital signal through its ADC module. The photo that depicts the setup is shown in Figure 4.2.

4.1.3 Experimental Results

Since the values of the coefficients α , β and γ affects the compensation performance, several experiments have been done to tune these values. As a result they are chosen to be 0.014, 1.1115 and -1.0387 respectively.

One of the several facts observed at the end of the experiments is the increase in the hysteretic behaviour as the travel range increases. In figure 4.3 part a) shows the results when the frequency of the voltage input is fixed as 1 Hz and the amplitude is changed.

Another fact is the increase in the hysteretic behaviour as the frequency increases. This is showed in figure 4.3 part b) where the amplitude of the voltage input is fixed as 2.5 and the frequency is changed.

When it comes to the compensation of the hysteretic behaviour, sinusoidal input frequency is set to 1 Hz which is an appropriate frequency value since applications

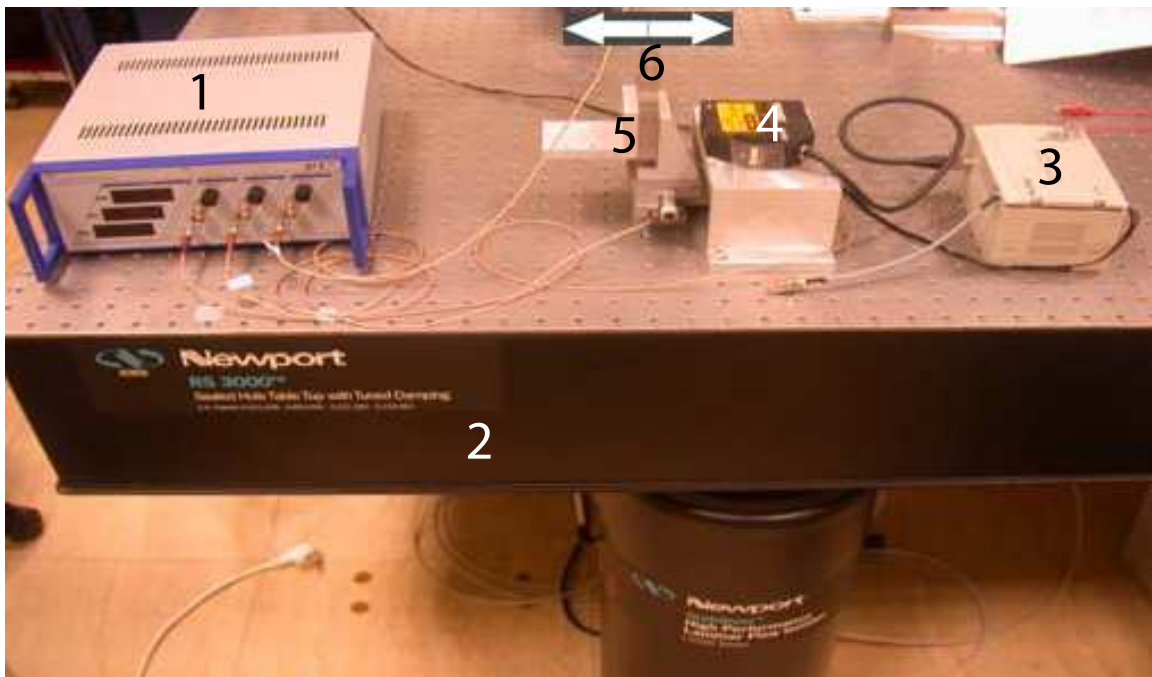


Figure 4.2: 1-PZT Amplifier, 2-Vibration Isolation Table, 3-Laser Controller, 4-Laser Head, 5-Three axis PZT actuator set, 6-Direction of movement

in micromanipulation requires slow motion. The compensation results are observed for different amplitudes. Figure 4.4 depicts the results in parts a), b) and c) for the amplitudes 20V, 50V and 80V respectively. Each graph include both the uncompensated and compensated loops. These results show the evident decrease in the hysteretic behaviour after compensation.

Figure 4.5 shows the position tracking results of the open loop controller that uses the compensated dynamics of the PZT actuator as reference tracking graph and error graph.(part a) and b) respectively)

4.2 Closed-loop Position Control of PZT Actuator using Sliding Mode Controller

Open loop control is applied as a first step towards the fulfillment of the task (namely high precision position control of PZT actuators) and it is used as the control algorithm during the hysteresis compensation efforts as explained above. However, it is not enough to obtain a reliable and long lasting control that handles all variations

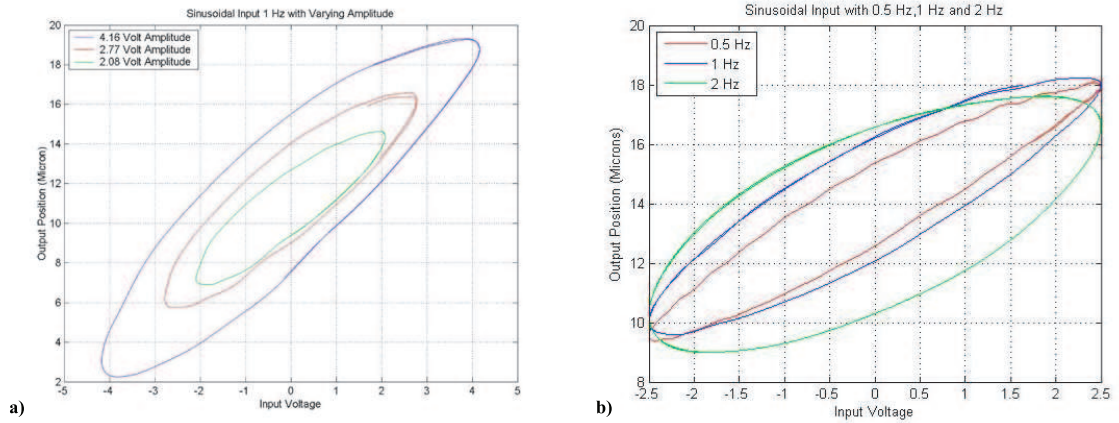


Figure 4.3: Results when sinusoidal voltage input is applied with a) Fixed frequency and varying amplitude, b) Varying frequency and fixed amplitude

happening in the system since without feedback, controller is not able to get the information about the state of the system and to act accordingly. Although good results are obtained in the sense of hysteresis compensation, it is not enough since there are other naturally nonlinear drawbacks of the system that have to be handled such as dead zone, backlash, saturation etc. Considering all these reasons, a discrete sliding mode control algorithm with disturbance observer has been designed and utilized to obtain high precision position control.

Sliding mode control is by definition characterized by a discontinuous control action that changes structure when it reaches a set of previously determined surfaces of switching. It is also known as a type of variable structure control (VSC). This attitude of the controller is very likely to end up with a successfully robust system which by the way provides a reliable high precision motion control.

4.2.1 Sliding Mode Controller Design

Taking a general system,

$$\dot{x} = f(x, t) + B(x, t)u(x, t) \quad x \in R^n, u \in R^m \quad (4.6)$$

knowing that $rank(B(x, t)) = m, \forall x, t > 0$ and all the elements of $f(x, t)$ vector, $B(x, t)$ matrix and their first order time derivatives are continuous and bounded, the control is defined by a discontinuous "u" as below;

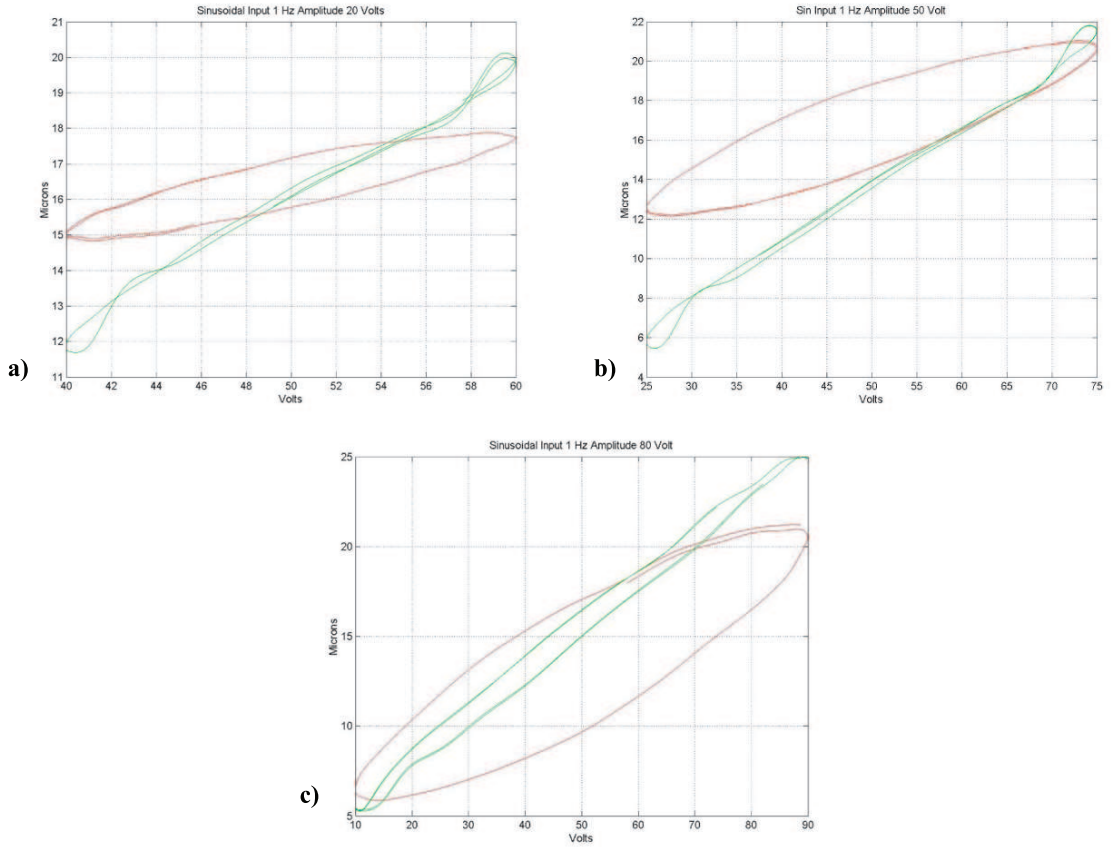


Figure 4.4: Results when sinusoidal voltage input is applied with 1 Hz frequency and a)20 V amplitude, b)50 V amplitude, c)80 V amplitude

$$u = \begin{cases} u^+(x, t), \sigma(x) > 0 \\ u^-(x, t), \sigma(x) < 0 \end{cases} \quad (4.7)$$

$$\sigma(x)^T = \{\sigma_1(x), \sigma_2(x), \dots, \sigma_m(x)\}, \sigma(x) = G(x^r - x) \quad (4.8)$$

where $u^+(x, t)$, $u^-(x, t)$ and $\sigma(x)$ are continuous functions, G is a positive integer chosen for the error converging response time and x^r is the reference position. The function $u(x, t)$ undergoes discontinuity on the manifold $\sigma(x) = 0$. (i.e. switching surface or switching hyperplane)

For this system definition of the sliding mode is given as below;

”Taking $S = X|_{\sigma(x)=0}$ as a switching surface including the point $x = 0$. For any

x_0 in S , if $x(t)$ is also in S for all $t > t_0$, then $x(t)$ is called as a sliding mode of the system. The switching surface S is called a sliding surface.”

In the vicinity of the switching surface S if the velocity vectors of the state trajectory are always towards the switching surface then the sliding mode exists.

4.2.2 Discrete Form

Since the controller is going to be operated using the data sampled at a specific frequency, design has to be able to work in a discrete manner. However, this discretization can create some shortcomings when the continuous-time algorithms are directly applied. On the other hand, a discontinuous-time algorithm is problematic to generate motion in a random manifold because of the switching frequency limitation by sampling frequency of the system. Chattering and instability may arise in these cases. This problematic is addressed by Drakunov and Utkin [43] and a continuous controller that can work for a discrete-time system is targeted. Their approach involves a design such that the system state reaches the predefined sliding manifold in finite time and then ”slides” along it.

Derivation of the Controller Structure

First of all we select a Lyapunov function $V(\sigma)$ making sure that both itself and the form of its derivatives $\dot{V}(\sigma)$ are going to satisfy the prerequisites for appropriate design.

A proper selection of this combination could be,

$$V(\sigma) = \frac{\sigma^2}{2} \tag{4.9}$$

$$\dot{V}(\sigma) = \sigma \dot{\sigma} \tag{4.10}$$

In our case let us select the derivative of the Lyapunov function as

$$\dot{V}(\sigma) = -D\sigma^2 - \mu \frac{\sigma^2}{|\sigma|} \tag{4.11}$$

where D and μ are positive constants, to guarantee the asymptotic stability of the solution $\sigma(x, x^r) = 0$ since $V(\sigma) > 0$, $V(0) = 0$ and $\dot{V}(\sigma) < 0$.

The following equation can be obtained,

$$\sigma(\dot{\sigma} + D\sigma + \mu \frac{\sigma}{|\sigma|}) = 0 \quad (4.12)$$

using equations (4.10) and (4.11). From here we can the part in the parenthesis and write as,

$$\dot{\sigma} + D\sigma + \mu \frac{\sigma}{|\sigma|} = 0 \quad (4.13)$$

The sliding function is derived as

$$\dot{\sigma} = G(\dot{x}^r - \dot{x}) = G\dot{x}^r - G\dot{x} \quad (4.14)$$

then, using the equation below

$$\dot{x} = f + Bu(t) \quad (4.15)$$

the equation (4.14) can be rewritten as

$$\dot{\sigma} = G\dot{x}^r - Gf - GBu(t) = GB(u_{eq} - u(t)) \quad (4.16)$$

which has the solution

$$u(t) = u_{eq} + (GB)^{-1}(D\sigma + \mu \frac{\sigma}{|\sigma|}) \quad (4.17)$$

Utilizing Euler's approximation the continuous u_{eq} can be rewritten in discrete form,

$$\frac{\sigma((k+1)T_s) - \sigma(kT_s)}{T_s} = GB(u_{eq}(kT_s) - u(kT_s)) \quad (4.18)$$

where $k = Z^+$ and T_s is the sampling time.

Then $u(t)$ is discretized as,

$$u(kT_s) = u_{eq}(kT_s) + (GB)^{-1}(D\sigma(kT_s) + \mu \frac{\sigma(kT_s)}{|\sigma(kT_s)|}) \quad (4.19)$$

Using equations (4.18) and (4.19), $u_{eq}(kT_s)$ can be deduced as,

$$u_{eq}(kT_s) = u(kT_s) + (GB)^{-1} \left(\frac{\sigma((k+1)T_s) - \sigma(kT_s)}{T_s} \right) \quad (4.20)$$

The current value of the equivalent control which is a continuous function can be approximated using the single-step backward value of $u_{eq}(kT_s)$,

$$u_{eq_{k-1}} = u_{k-1} + (GB)^{-1} \left(\frac{\sigma_k - \sigma_{k-1}}{T_s} \right) \quad (4.21)$$

The resulting control structure as be written as,

$$u_k = u_{k-1} + (GBT_s)^{-1} \left((DT_s + 1)\sigma_k - \sigma_{k-1} + \mu \frac{\sigma(k)}{|\sigma(k)|} \right) \quad (4.22)$$

4.2.3 Disturbance Observer

A disturbance compensation is necessary to cope with the drawbacks of the system such as hysteresis, dead zone, saturation, backlash, time delay etc. as explained before. This compensation is done by combining all these effects in the model and lump them into a disturbance variable as a part of the plant response. Controller output changes in a way that it also takes this lumped effect into the picture. The method proposes this kind of design is also called as disturbance observing.

Assuming that all the external disturbances and inherent nonlinearities can be taken as a single disturbance variable, an observer is structured based upon the Eqn.(4.4) which involves the electromechanical structure of the PZT actuator.

$$\begin{aligned} m_p \ddot{x} + c_p \dot{x} + k_p x &= T_p u(t) - F_{dis} \\ F_{dis} &= T_p H + \Delta T(v_p + v_h) + \Delta m \ddot{x} + \Delta c \dot{x} + \Delta k x \end{aligned} \quad (4.23)$$

Here, in addition to the plant parameters m_p , c_p , k_p and T_p (which corresponds to T_{em}) that also exists in the Eqn.(4.4), there exist Δm , Δc , Δk and ΔT as the relevant uncertainties. Moreover, $(v_p + v_h)$ corresponds to u_{in} in the Eqn.(4.4).

Measurable quantities are x as the displacement and u_t as the input. Observer can be structured as below regarding these quantities,

$$m_p \ddot{\hat{x}} + c_p \dot{\hat{x}} + k_p \hat{x} = T_p u - T_p u_c \quad (4.24)$$

where \hat{x} is estimated position, $\dot{\hat{x}}$ is estimated velocity and $\ddot{\hat{x}}$ is estimated acceleration are represented by \hat{x} , $\dot{\hat{x}}$ and $\ddot{\hat{x}}$ respectively. The input from the observer control is represented by u_c .

Estimated position should successfully follow the measured position (\hat{x} and x respectively) when estimated velocity also follows measured velocity ($\dot{\hat{x}}$ and \dot{x} respectively) in order to say that the observer is working well. That's why the sliding manifold (σ_{obs}) is dependent upon the differences between these estimated and measured values.

$$\sigma_{obs} = \lambda_{obs}(y - \hat{y}) + (\dot{y} - \dot{\hat{y}}) \quad (4.25)$$

where λ_{obs} is a coefficient which is positive. Here \hat{y} has to go to y in order to make σ_{obs} go to zero.

Equation below is written,

$$\dot{\sigma}_{obs} + D_{obs}\sigma_{obs} = 0 \quad (4.26)$$

where the condition $\sigma_{obs} \rightarrow 0$ is guaranteed. Modifying it we can write,

$$(\ddot{y} - \ddot{\hat{y}}) + (\lambda_{obs} + D_{obs})(\dot{y} - \dot{\hat{y}}) + \lambda_{obs}D_{obs}(y - \hat{y}) = 0 \quad (4.27)$$

as the resulting equation.

The roots of the closed-loop system are $-\lambda_{obs}$ and $-D_{obs}$ and the controller structure of the observer will be same with the one in Eqn.(4.22).

Using the input matrix derived from Eqn.(4.24) and the matrix G as below,

$$B_{obs} = \begin{bmatrix} 0 & -\frac{T_p}{m_p} \end{bmatrix}^T \quad (4.28)$$

$$G = [\lambda_{obs} \quad 1] \quad (4.29)$$

the compensated control input is obtained as,

$$u_{c_k} = u_{c_{k-1}} - \frac{m_p}{T_p} \left(D_{obs}\lambda_{obs_k} + \frac{\sigma_{obs_k} - \sigma_{obs_{k-1}}}{T_s} \right) \quad (4.30)$$

4.2.4 Implementation on PZT and Experimental Results

One axis of a 3-axis *PhysikInstrumente^{PI}* piezo-stage driven by E-664 power amplifier is used to validate the usefulness of the designed controller with the disturbance observer.

dSpaceTM 1103 data acquisition board is used as the signal interface between the piezo-stage and computer where the algorithm coded in C can operate to realize the control action.

Verification of the performance of the controller is obtained using step, trapezoidal and sinusoidal position reference inputs to the system. Figure 4.6 part a), b) and c) depicts the 50nm step, 0.5 μm height trapezoidal and 1 μm amplitude, 0.5Hz frequency sinusoidal input responses.

The steady state error was 2% and the rise time was 23ms for 50 nanometer step input, without any overshoot which is important since the overshoot must be avoided in such sensitive manipulation applications. On the one hand the probe can hit the surface that holds micro objects and can get damaged. On the other hand, the micro object that is being manipulated may be fragile and easily pierceable which creates another problem. For 0.5 μm height trapezoidal input response tracking error is found to be less than $\pm 10 nm$ again without any overshoot. Lastly, for the sinusoidal input which has 1 μm amplitude and 0.5Hz frequency, the tracking error was within $\pm 20 nm$.

These values show that an enough high precision position control is obtained. The only problem is a little noise seen in steady state parts of the measurements. The main source of this noise was the electronic devices and interfaces connected to the computer. Although some modifications have been made to compensate that, some of it remained as it was.

4.3 Conclusion

In the work explained in this chapter, nanometer precision motion control of PZT actuator is realized first as open-loop control, then as closed loop control using discrete-time sliding mode controller with disturbance observer. Hysteresis com-

compensation for PZT actuator motion is achieved using an appropriately developed model and the results of the open-loop control experiments showed that the hysteresis effect could be canceled. Then a discrete-time sliding mode controller is formulated and implemented along with a disturbance observer to control the piezoelectric actuators position in a closed-loop fashion. Experimental results showed that a sufficient high precision position control is obtained with no overshoot.

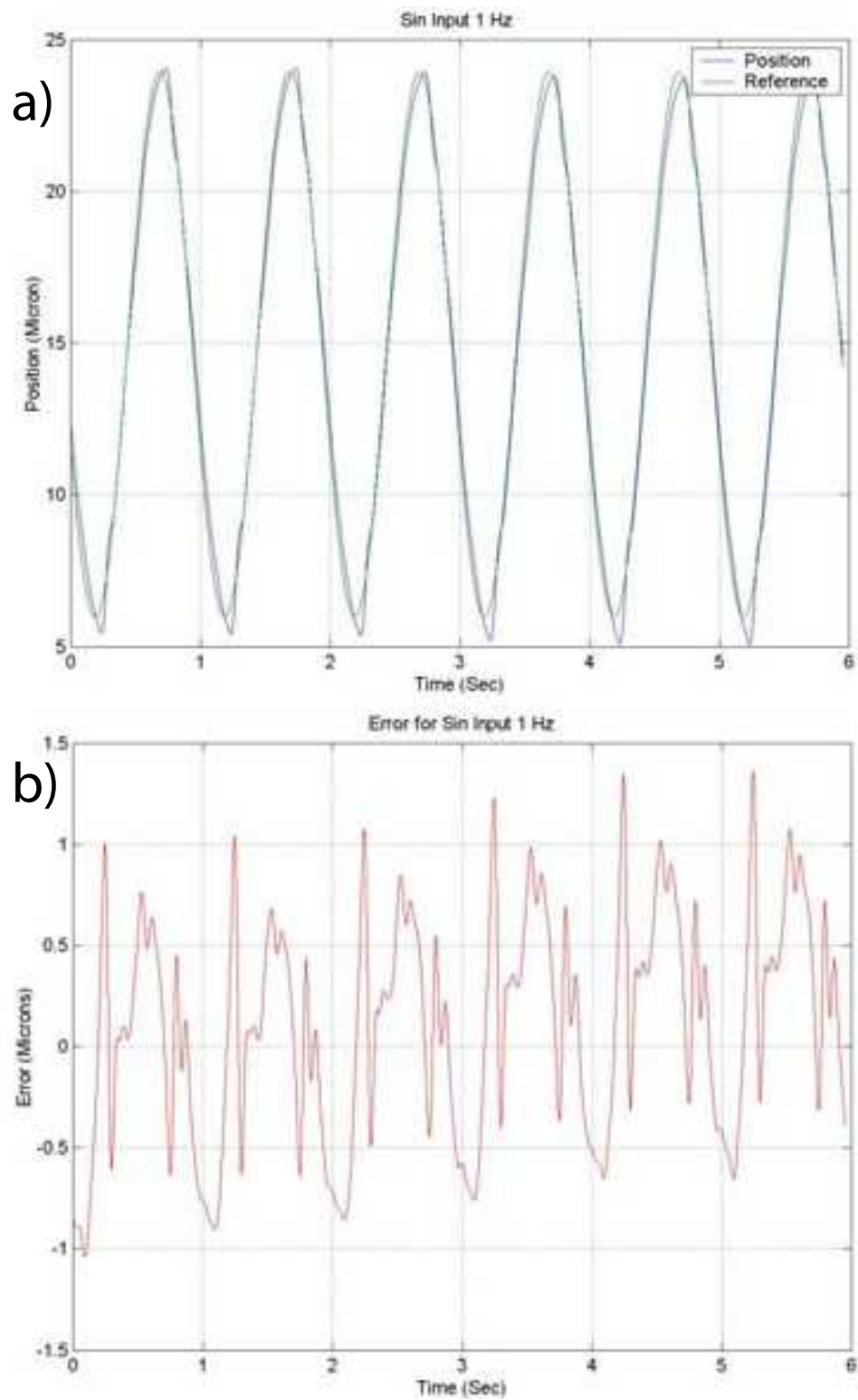


Figure 4.5: a)Reference tracking for sinusoidal input, b)Error of reference tracking for sinusoidal input

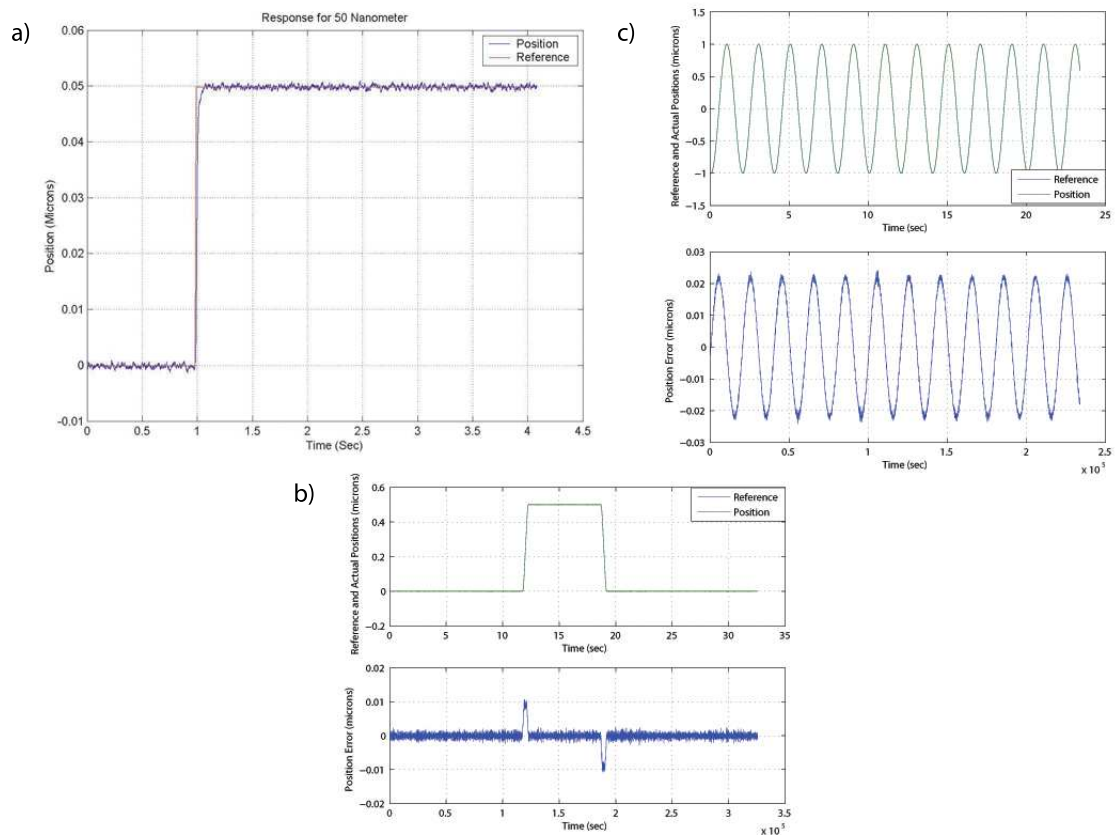


Figure 4.6: a) Position response for a reference of $50nm$ [1], b) Position response for a trapezoidal reference with height $0.5 \mu m$, c) Position response for a sinusoidal reference with $1\mu m$ amplitude and $1Hz$ frequency

Chapter 5

Scaled Bilateral Teleoperation for Micro-manipulation by Pushing in 1-D

As explained before the improvement in the 1-D micro pushing mechanism was planned to be achieved via integrating the human into the pushing process as the one who operates the process. Since human can not have the direct access to the micro scale environment, utilization of a bilateral controller between the micro scale where the manipulation takes place and the macro level to where the human operator has access, became inevitable. The position of the master actuator operated by the human is scaled by a factor α and sent to the controller mechanism of the piezoelectric actuator in slave side when the slave side's 1-D environmental interaction force is scaled by a factor β and fed back to the mechanism that controls the master actuator. Actually these two mechanisms work in the same structure called as bilateral controller. Two different schematics of the same system is shown in Figure 5.1.

As mentioned in [30], the essential desire in the bilateral teleoperator system design is to provide a loyal transmission of signals (positions, velocities, forces) between master and slave to couple the operator as closely as possible to the remote task. In ideal case, complete transparency must be obtained in the teleoperation system. This means that the operator can feel like he/she is directly interacting with the

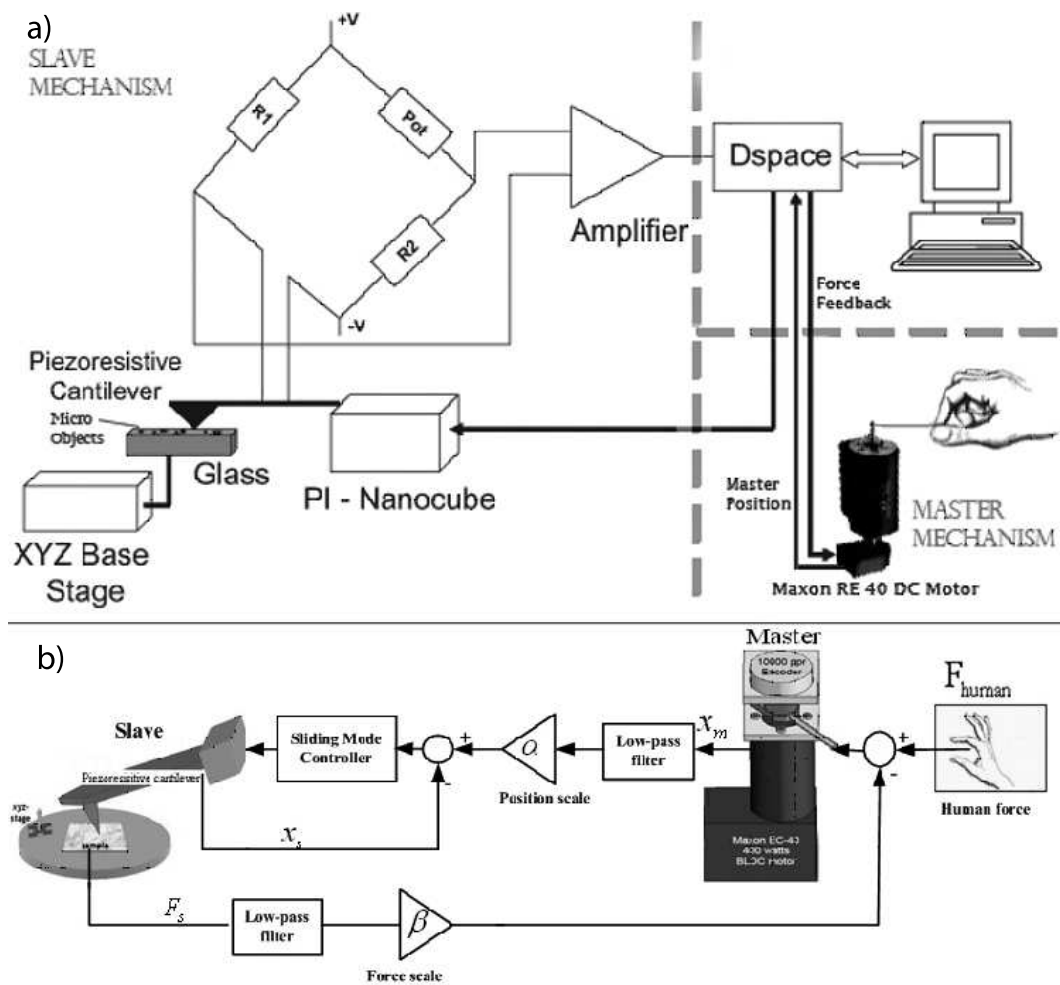


Figure 5.1: Schematics of the bilateral system

remote task [31] which corresponds to slave side environment. Accepting the fact that the full transparency is just an ideal condition, adjustment of the scaling factors of the system mentioned above, must be done in a way that the transparency can be obtained along with the satisfaction of operator requirements.

Oscillatory behavior is observed both in master and slave system because of the human hand and piezoresistive cantilever properties respectively. Low pass filtering has been applied to suppress this oscillation before scaling.

5.1 Nano-Newton Force Sensing

Regarding the micro scale where the targeted manipulation by pushing is happening, accurate measurement of the interaction force was necessary in order to obtain

successful control over that scale. Measurements has been done utilizing a piezoresistive microcantilever along with an integrated Wheatstone bridge and a lightly doped strain gauge which is produced by Applied Nanostructures as a whole. When there is an applied force on the free end of the cantilever, it makes cantilever bend and this deflection is sensed as a resistance change in a part of Wheatstone bridge since cantilever stands as one of the resistors of the bridge. There was a disagreement between the resistance values of the resistors within the Wheatstone bridge although they were claimed to be equal and to satisfy the balanced zero voltage output from the Wheatstone bridge. This problem is solved connecting a potentiometer to the circuit and the balance is obtained. The amount of deflection is measured considering the voltage output of the Wheatstone bridge. The output voltage which has a range of ± 20 V, is amplified to make it fit to the input range of data acquisition module of the dSpace controller board which is ± 10 V.

Hooke's Law is used for the force calculation;

$$F = K_c z \quad (5.1)$$

where K_c and z are the spring constant and the deflection respectively. Linear beam equation is used to calculate the spring constant;

$$K_c = \frac{3EI}{L^3} \quad (5.2)$$

where E is the modulus of elasticity for silicon (190GPa), L is the length of the microcantilever ($298.98\mu\text{m}$) and I is the moment of inertia that can be calculated by;

$$I = \frac{bh^3}{12} \quad (5.3)$$

where b is the width of the microcantilever ($50\mu\text{m}$) and h is the height of microcantilever ($1.6\mu\text{m}$). As a result K_c is calculated as $0.3603\frac{\text{N}}{\text{m}}$.

5.1.1 Experimental Results and Validation

For the experiments the cantilever is mounted to the three axes closed loop controlled piezo stage. A glass slide is placed on the way of the tip of the cantilever. Verification of the force sensing ability has been obtained by making the tip approach to the glass slide and the change in the measured force is observed because of the attractive forces between the tip and glass slide. Results in part a) of the Figure 5.2 depicts that the measured force is increasing as the position of the tip increases starting from the reference point and going towards the glass slide. Moreover, verification of the value of the measured force has been obtained by comparing it to the theoretical value. For this pull-off force between the tip and the glass slide surface is taken as an example. Dugdale model [44] approximation to the interaction forces between spherical tips and planar surfaces has been used for finding the theoretical value of the pull-off force. Calculation of the force is done as below;

$$F_{pull-off} = \left(\frac{7}{4} - \frac{1}{4} \frac{4.04\lambda^{\frac{1}{4}} - 1}{4.04\lambda^{\frac{1}{4}} + 1} \right) \pi W R \quad (5.4)$$

where R is the sphere radius, W is the work of adhesion between silicon and glass mediums and λ is the coefficient that corresponds to the utilized contact model for a any case(here $\lambda = 0.54$). Using this model, the calculated force is 39.43 nN [45, 46]. Figure 5.2 part b) shows the result of the experimental measurement of the pull-off force which is determined as 40 nN . This is almost same with the theoretically found value.

5.2 Position/Force Tracking on Master and Slave

As explained before, the success of the bilateral structure depends on the appropriate scaling of the transferred signals between the master and slave sides which are in different scales. Here position and force signals are being transferred from master side to slave side and slave side to master side respectively. Equations below govern the scaling between these sides.

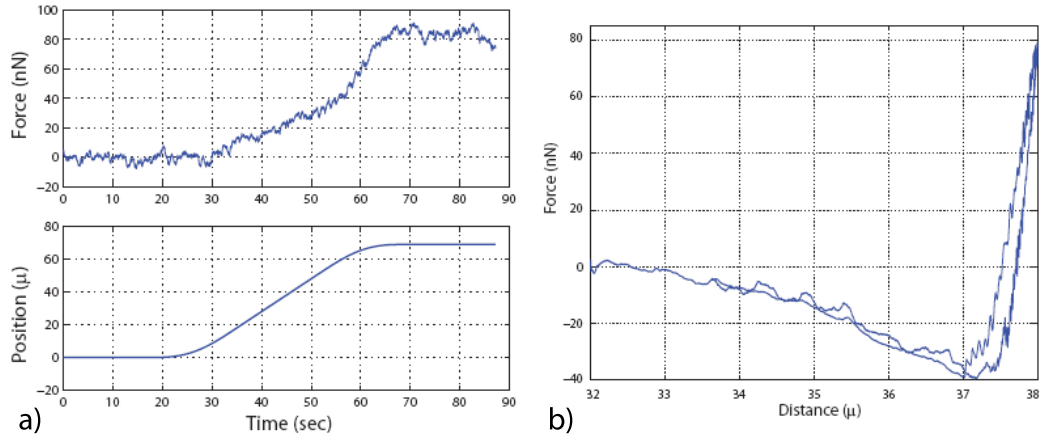


Figure 5.2: Force Sensing Results a) Approaching mode b) Pull-off mode

$$\begin{aligned} x_s &= \alpha x_m \\ F_m &= \beta F_s \end{aligned} \quad (5.5)$$

Here x_m and F_m are the position and force of the master side. Similarly, x_s and F_s denotes the position and force of the slave side. Accordingly, α is the scaling factor of position where β is the scaling factor of force.

Operational needs determine the parameters that guide the tuning process of the scaling factors. Smooth and slow motion of the slave side corresponding to the more rough movements of master side was the first target. The ratio chosen was $1\mu m$ linear displacement of slave side actuator per $360deg$ angular displacement of master actuator. Corresponding scaling factor was $\alpha = 0.0027 \frac{\mu m}{deg}$. Then force scaling has been tuned depending on the feedback from the human operator regarding the measured slave forces. The criterion was the tangibility of the forces by the operator. This practical tuning process ended with the scaling factor $\beta = 0.00366 \frac{N}{nN}$ which corresponds to a $1N$ applied force on the master side for every $0.00366nN$ force measured as the applied force on the tip at the slave side.

5.2.1 Experimental Results and Validation

Figure 5.3 depicts the position and force tracking results in parts a) and b) respectively. In the first part, there exist two graphs. Upper graph shows the master and slave position measurement on top of each other, where the master position

signal is depicted after scaling down to the slave position level. This is made just in order to see them on top of each other which gave a better intuition about the tracking performance. Lower graph shows the position tracking error. It is clearly observable that the slave position is tracking the master position almost accurately. This result is satisfying for the micro scale positioning purposes since the tracking error is within $\pm 2nm$ where the movement is within $\pm 20nm$.

In the second part of the Figure 5.3 again there exist two graphs. Upper graph shows the master and slave force measurement on top of each other, where the slave force signal is depicted before scaling up to the master force level. This is also made in order to see them on top of each other for a better intuition about the tracking performance. Lower graph shows the force tracking error. When the values from the two graphs are compared, the error found to be around %3 which implies that the master force is tracking the slave force with a good precision that is enough for the targeted micro pushing application. As one can also understand from the scale of the upper graph, values in these graphs are not exactly the force values measured but scaled versions of them since it is easier to see the error percentage with scaled values.

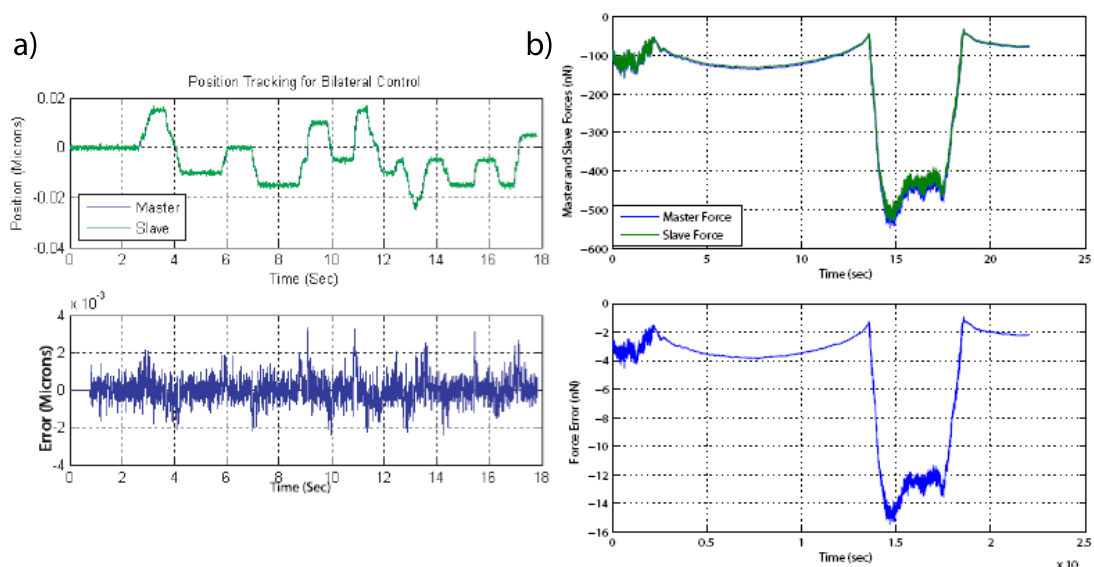


Figure 5.3: a) Position and b) Force Tracking Results

5.3 Conclusion

In this chapter the development and verification of the necessary components of scaled bilateral teleoperation for micro pushing are presented. Firstly, the method to obtain nano-Newton scale force sensing is explained and the relevant results taken via applying this method are shown. These results proved that the applied interaction force on the slave side manipulator can be sensed effectively. Secondly, the bilateral structure and the position and force tracking between master and slave sides are explained. Again experimental results have been used to show that the transparency could be obtained between master and slave sides. In other words the human operator on the master side could get the feeling of the forces on the slave side scaled up to the level that human can sense.

Chapter 6

Conclusion

6.1 Summary of the Thesis

In this work, the target of the project was obtaining an improved performance in 1-D pushing of micrometer scaled objects and it is tried to be achieved via developing a custom micromanipulation setup that has the ability of nano-Newton scale force sensing and combining it with a bilateral control structure which uses discrete sliding mode controller with disturbance observer which is again designed for the actuators of the custom made system. The bilateral structure was for allowing human operator to intervene more to the pushing process.

The steps that are targeted and accomplished during the process can be listed as below;

- Development of a closed loop sliding mode controller with disturbance observer to obtain high precision control of piezo actuators.
- Achievement of force sensing in nano-Newton scale by using a piezoresistive cantilever with inbuilt wheatstone bridge.
- Application of a bilateral architecture to the previously developed closed loop controller and achievement of almost full transparent position and force tracking using this combined structure.
- Combination of these facilities in a custom made micromanipulation setup for

bilaterally operated 1-D pushing experience.

Improvement of 1-D pushing mechanism comparing to the ones in literature is mainly based upon the bilateral structure which can be tuned by the user according to the objective and more importantly it allows human intervention to the pushing process as an operator.

The nano-Newton scale force sensing ability of the system lets user to utilize this as a force feedback within the bilateral structure which makes the operator understand when the piezoresistive cantilever beam touched the object that is going to be pushed by it. Moreover, the operator understands when there is an obstacle or opposite force that keeps the object from continuing on its track. The best property of this facility is that the calibration can be done in a way that will make the system very sensitive. A really small force in nano-Newton scale can be transferred to the master side as a tangible force. In other words sensitivity of the force transfer from slave side to the master side of the system is tunable.

Sensitivity of the position transfer within the bilateral structure is another tunable entity. However this time it is from master side to slave side. This ability to calibrate the relation between the cycle that is made by the DC motor shaft which is controlled by the operator and the movement of the slave system makes the slower and smoother motion of the slave actuator obtainable. For this, calibration must be done in a way that less distance is gone by the slave actuator per the cycle made by the master actuator.

6.2 Problems and Future Works

Several problematic issues created some drawbacks during the project. One of them was the disagreement of the resistance values of the resistors within the Wheatstone bridge which is built in the utilized piezoresistive cantilever. They were claimed to be equal and to satisfy the balanced zero output from the Wheatstone bridge but actual values were not exactly equal. Although the differences were really small this situation was creating a problem considering the voltage output of the bridge which is in millivolt scale. In order to cope with this problem a potentiometer is connected

to the circuit and the balance is obtained. However, this created another drawback because potentiometer was drifting from the set value after every experiment. Usage of a digital potentiometer was proposed as a solution of this problem but has not been applied.

Another imperfection of the process was in the sense of the deflection model used for the piezoresistive cantilever. Cantilever is modeled as a spring and the calculations were based on the spring model with a spring constant obtained from the producer of the cantilever. However, actual deflection is different and a possible improvement in this model could increase the accuracy of the measured forces.

In addition to these, the setup was in the room environment and was not isolated from the room conditions. So the humidity in the room was effecting the results since capillary forces exist as a dominant factor in micro scale contact mechanics. As a solution to this problem, isolation of the setup in a vacuum environment can be proposed for the ones who will build a similar project setup for micro/nano-manipulation purposes.

Last shortage was resulted from the type of the microscope used. Since an optical microscope with old-school objectives is used as the imaging device, the magnification could not be set more than 20x although objectives with more than 20x magnification were existing. The reason was the decrease in the working distance when the magnification increases. Even with 20x magnification, objective was so close and almost touching to the piezoresistive cantilever pad which is something undesired for the proper operation of the cantilever and inbuilt wheatstone bridge.

As an application and future work of the project, manipulation and mechanical characterization of biological cells can be proposed. however before embarking into this application the setup built in this project must be modified in a way that the nano-Newton force sensing mechanism can work in liquids which will be including the living cells. In other words, the circuit on the mechanism should has to be isaolated in a way that it will not touch the liquid not to create a short circuit.

Bibliography

- [1] S. Khan, M. Elitas, E. D. Kunt, and A. Sabanovic, “Discrete sliding mode control of piezo actuator in nano-scale range,” in *IEEE/ICIT International Conference on Industrial Technology*, 2006.
- [2] R. P. Feynman, “There is plenty of room at the bottom,” in *Annual meeting of the American Physical Society*, 1959.
- [3] F. Arai, D. Ando, and T. Fukuda, “Micromanipulation based on micro physics: Strategy based on attractive force reduction and stress measurement,” in *IEEE/RSJ International Conference on Robotics and Automation*, pp. 236–241, 1995.
- [4] S. Johansson, “Micromanipulation for micro and nano manufacturing,” in *Proceedings 1995 INRIA / IEEE Symposium on Emerging Technologies and Factory Automation*, vol. 3, pp. 3–8, 1995.
- [5] A. Codourey, W. Zesch, R. Buechi, and R. Siegwart, “A robot system for automated handling in micro-world,” in *Proceedings IEEE/RSJ Intelligent Robots and Systems*, pp. 185–190, 1995.
- [6] J. T. Feddema and R. W. Simon, “Visual servoing and cad-driven microassembly,” in *IEEE Robotics and Automation Magazine*, vol. 5, pp. 18–24, 1998.
- [7] T. Kasaya, H. Miyazaki, S. Saito, and T. Sato, “Micro-object handling under sem by vision-based automatic control,” in *SPIE Conference on Microrobotics and Micromanipulation*, vol. 3519, pp. 181–188, 1998.

- [8] B. J. Nelson, Y. Zhou, and B. Vikramaditya, "Sensor-based microassembly of hybrid mems devices," in *IEEE Control Systems Magazine*, vol. 18, pp. 35–45, 1998.
- [9] A. Pillarisetti, M. Pekarev, A. D. Brooks, and J. P. Desai, "Evaluating the role of force feedback for biomanipulation tasks," in *14th Symposium on Haptic Interfaces for Virtual Environment and Teleoperator Systems*, pp. 11–18, 2006.
- [10] D. Kim, S. Yun, and B. Kim, "Mechanical force response of single living cells using a microrobotic system," in *Proceedings of the 2004 IEEE International Conference on Robotics and Automation*, vol. 5, pp. 5013–5018, 2004.
- [11] A. Pillarisetti, W. Anjum, J. P. Desai, G. Friedman, and A. D. Brooks, "Force feedback interface for cell injection," in *Proceedings of the First Joint Eurohaptics Conference and Symposium on Haptic Interfaces for Virtual Environment and Teleoperator Systems*, pp. 391–400, 2005.
- [12] Y. Shen, N. Xi, and W. J. Li, "Contact and force control in microassembly," in *Proceedings of the 5th IEEE International Symposium on Assembly and Task Planning*, pp. 60–65, 2003.
- [13] A. Ferreira, C. Cassier, and S. Hirai, "Automatic microassembly system assisted by vision servoing and virtual reality," in *IEEE/ASME Transactions on Mechatronics*, vol. 9, pp. 321–333, 2004.
- [14] H. Hashimoto and M. Sitti, "Challenge to micro/nanomanipulation using atomic force microscope," in *Proceedings of 1999 International Symposium on Micromechatronics and Human Science*, pp. 35–42, 1999.
- [15] Z. Lu, P. C. Y. Chen, J. Nam, R. Ge, and W. Lin, "A micromanipulation system with dynamic force-feedback for automatic batch microinjection," in *Journal of Micromechanics and Microengineering*, vol. 17, pp. 314–321, 2007.
- [16] M. Sitti, S. Horiguchi, and H. Hashimoto, "Nano tele-manipulation using virtual reality interface," in *Proceedings of IEEE International Symposium on Industrial Electronics, ISIE'98*, vol. 1, pp. 171–176, 1998.

- [17] S. Fahlbusch and S. Fatikow, "Micro force sensing in a micro robotic system," in *Proceedings of the 2001 IEEE International Conference on Robotics and Automation*, vol. 4, pp. 3435–3440, 2001.
- [18] C. Baur, A. Bugacov, B. Koel, A. Madhukar, N. Montoya, T. Ramachandran, A. Requicha, R. Resch, and P. Will, "Nanoparticle manipulation by mechanical pushing: Underlying phenomena and real-time monitoring," in *Nanotechnology*, vol. 9 of 4, pp. 360–364, 1998.
- [19] K. Lynch, "The mechanics of fine manipulation by pushing," in *Proceedings of IEEE International Conference on Robotics and Automation*, vol. 3, pp. 2269–2276, 1992.
- [20] M. Sitti, "Atomic force microscope probe based controlled pushing for nano-tribological characterization," *IEEE/ASME Transactions on Mechatronics*, vol. 9, no. 2, 2004.
- [21] M. Sitti and H. Hashimoto, "Force controlled pushing of nanoparticles: Modeling and experiments," in *Proceedings of IEEE International Conference on Advanced Intelligent Mechatronics*, pp. 13–20, 1999.
- [22] A. de Lazzer, M. Dreyer, and H. J. Rath, "Particle-surface capillary forces," in *Langmuir*, pp. 4551–4559, 1999.
- [23] M. He, A. Szuchmacher-Blum, D. E. Aston, C. Buenviage, R. M. Overney, and R. Luginbhl, "Critical phenomena of water bridges in nanoasperity contacts," in *Journal of Chemical Physics*, vol. 114 of 3, pp. 1355–1360.
- [24] M. Sitti, S. Horiguchi, and H. Hashimoto, "Nano tele-manipulation using virtual reality interface," in *Proceedings ISIE '98 IEEE International Symposium on Industrial Electronics*, pp. 171–176, 1998.
- [25] M. Sitti and H. Hashimoto, "Teleoperated touch feedback from the surfaces at the nanoscale: Modeling and experiments," in *IEEE/ASME Transactions on Mechatronics*, vol. 8 of 1, pp. 287–298, 2003.

- [26] D. H. Kim, Y. Kim, K. Y. Kim, and S. M. Cha, "Dexterous teleoperation for micro parts handling based on haptic/visual interface," in *IEEE International Symposium in Micromechatronics*, pp. 211–217, 2001.
- [27] D.Kim, K.Kim, and K.Kim, "A micro manipulation system based on teleoperation techniques," in *Proceedings of the 32nd ISR(International Symposium on Robotics)*, 2001.
- [28] N.Ando, M.Ohta, K.Gonda, and H.Hashimoto, "Micro teleoperation with parallel manipulator," in *2001 IEEE/ASME International Conference on Advanced Intelligent Mechatronics Proceedings*, pp. 63–68, 2001.
- [29] C.D.Onal, C.Pawashe, and M.Sitti, "A scaled bilateral control system for experimental 1-d teleoperated nanomanipulation applications," in *IEEE/RSJ International Conference on Intelligent Robots and Systems, IROS 2007*, pp. 483–488, 2007.
- [30] D. Lawrence, "Stability and transparency in bilateral teleoperation," in *IEEE Transactions on Robotics and Automation*, vol. 9 of 5, pp. 624–637, 1993.
- [31] G. Raju, G. Verghese, and T. Sheridan, "Design issues in 2-port network models of bilateral remote teleoperation," in *Proceedings of IEEE International Conference on Robotics and Automation*, pp. 1317–1321, 1989.
- [32] S.Katsura, Y.Matsumoto, and K.Ohnishi, "Realization of "law of action and reaction" by multilateral control," in *IEEE Transaction in Industrial Electronics*, vol. 52 of 5, pp. 1196 – 1205, 2005.
- [33] H.Adriaens, W. L. de Koning, and R.Banning, "Modeling piezoelectric actuators," in *Journal of Mechatronics*, vol. 5, pp. 331–341, 2000.
- [34] Y.Stepanenko and C.Y.Su, "Intelligent control of piezoelectric actuators," in *In Proceedings of the 37th IEEE Conference on Decision and Control*, vol. 4, pp. 4234–4239, 1998.
- [35] D.Song and C.J.Li, "Modeling of piezo actuator's nonlinear and frequency dependent dynamics," in *Journal of Mechatronics*, vol. 4, pp. 391–410, 1999.

- [36] M. A. Krasnoselski and A. V. Pokrovski, "Systems with hysteresis," (Moscow), Nauka, 1983.
- [37] K. Kuhnen and H. Janocha, "Real-time compensation of hysteresis and creep in piezoelectric actuators," in *Journal of Sensors and Actuators*, vol. 7 of 9, pp. 83–89, 2000.
- [38] M. Goldfarb and N. Celanovic, "Modeling piezoelectric stack actuators for control of micromanipulation," in *IEEE Control Systems Magazine*, vol. 17, pp. 69–79, 1997.
- [39] B. J. Lazan, "Damping of materials and members in structural mechanics," in *Pergamon*, 1968.
- [40] Y.K.Wen, "Method for random vibration of hysteretic systems," in *Journal of Engineering and Mechanics*, vol. 102, pp. 249–263, 1976.
- [41] M.C.Constantinou and I.G.Tadjbakhsh, "Hysteretic dampers in base isolation: Random approach," in *Journal of Structural Engineering*, pp. 705–721, 1998.
- [42] C.P.Heine, "Simulated response of degrading hysteretic joints with slack behavior," in *Ph.D. dissertation*, Virginia Polytechnic Institute and State University, 2001.
- [43] S. V. Drakunov and V. Utkin, "A semigroup approach to discrete-time sliding modes," in *Proceedings of the American Control Conference*, pp. 1314–1317, 1995.
- [44] K. L. Johnson, *A Continuum Mechanics Model of Adhesion and Friction in a Single Asperity Contact: In Micro-Nanotribology and Its Applications*. Kluwer Academic Publishers, 1997.
- [45] M. Sitti and R. Fearing, "Synthetic gecko foot-hair micro-nanostructures as dry adhesives," in *Journal of Adhesion Science Technology*, vol. 17 of 8, pp. 1055–1073, 2003.

- [46] P. Rougeot, S. Regnier, and N.Chaillet, “Force analysis for micromanipulation,” in *IEEE CIRA*, pp. 105–110, 2005.

Appendix A

Tele-Micromanipulation Setup

Table A.1: Maxon RE 40 DC Motor Data

| | |
|--|------------------|
| <i>Nominal voltage</i> | V |
| <i>No load speed</i> | rpm |
| <i>No load current</i> | mA |
| <i>Nominal speed</i> | rpm |
| <i>Nominal torque (max. continuous torque)</i> | mNm |
| <i>Nominal current (max. continuous current)</i> | A |
| <i>Stall torque</i> | mNm |
| <i>Starting current</i> | A |
| <i>Max. efficiency</i> | % |
| <i>Terminal resistance</i> | Ω |
| <i>Terminal inductance</i> | mH |
| <i>Torque constant</i> | mNm / A |
| <i>Speed constant</i> | rpm / V |
| <i>Speed / torque gradient</i> | rpm / mNm |
| <i>Mechanical time constant</i> | ms |
| <i>Rotor inertia</i> | gcm ² |

Table A.2: Maxon 4-Q-DC Servoamplifier Data

| | |
|---------------------------------------|------------------------------|
| Supply voltage V_{CC} | 12 - 50 VDC |
| Max. output current I_{max} | 10 A |
| No load current | mA |
| Continuous output current I_{cont} | 5 A |
| Switching frequency of power stage | 50 kHz |
| Efficiency | 95 % |
| Band width current controller | 2.5 kHz |
| Built-in motor choke | 160 μ H / 5 A |
| Input | |
| Set value | -10 ... +10 V |
| Enable | +4 ... +50 V |
| Input voltage DC tachometer | 2 VDC - 50 VDC |
| Encoder signals | max. 100 kHz, TTL |
| Output | |
| Current monitor "Monitor I" | -10 VDC ... +10 VDC |
| Speed monitor "Monitor n" | -10 VDC ... +10 VDC |
| Status reading "READY" | max. 30 VDC |
| Voltage output | |
| Aux. voltage, short circuit protected | +12 VDC, -12 VDC, max. 12 mA |
| Encoder supply voltage | +5 VDC, max. 80 mA |

Table A.3: Maxon Choke Module Technical Data

| | |
|---|-----------------------------|
| Electrical data per linear storage choke | |
| Nominal DC current | $I_N = 10\text{A}$ |
| Inductance at I_N | $L = 150\mu\text{H}$ |
| DC current resistance | $R_{Cu} = 24\text{m}\Omega$ |
| Max. current ripple | $\Delta I = 0.2 \cdot I_N$ |
| Temperature range | -25...70°C |
| Humidity range | 20...75% non condensating |
| Mechanical data of choke module | |
| Weight: | 250g |
| Dimensions: | 90mm x 70mm x 49mm |
| Mounting plate: | for 4 screws M3 |
| Distance between threads: | 80 x 54mm |
| Connections | |
| PCB clamps | 4-polig |
| Pitch suitable for cable profile | 5.08mm |
| multiplestranded wire | 0.14...2.5mm ² |
| single wire | 0.14...4.0mm ² |

Appendix B

Nano-meter Precision Motion Control of PZT Actuator

Table B.1: Specifications of Piezo-Stage

| Symbol | Quantity | Value in SI |
|----------|----------------------|-------------------------|
| m_p | Nominal Mass | $1.5 \times 10^{-3} Kg$ |
| c_p | Nominal Damping | $220 \frac{Ns}{m}$ |
| k_p | Nominal Stiffness | $300000 \frac{N}{m}$ |
| f_r | Resonant Frequency | $350 Hz$ |
| T_{em} | Transformation Ratio | $0.3 \frac{N}{V}$ |